FRIEDRICH-SCHILLER-UNIVERSITÄT JENA
PHYSIKALISCH-ASTRONOMISCHE-FAKULTÄT

FRIEDRICH-SCHILLER-
UNIVERSITÄT
JENA

WINTERSEMESTER 2021/2022

Quantum Imaging and Sensing

MARKUS GRÄFE, FRANK SETZPFANDT

LaTeX-Satz und Design von Martin Beyer

Contents

1 Fundamentals of Quantum Optics

1.1 Field quantization in a nutshell

We start our discussion with MAXWELL's field equations for free space

$$\vec{\nabla} \times \boldsymbol{E} = -\frac{\partial \boldsymbol{B}}{\partial t} \qquad \vec{\nabla} \cdot \boldsymbol{E} = 0 \tag{1.1}$$

$$\vec{\nabla} \times \boldsymbol{B} = \mu_0 \varepsilon_0 \frac{\partial \boldsymbol{E}}{\partial t} \qquad \vec{\nabla} \cdot \boldsymbol{B} = 0. \tag{1.2}$$

A possible solution of this set of equations is

$$E_x(z,t) = \sqrt{\frac{2\omega^2}{V\varepsilon_0}} q(t) \sin(kz) \tag{1.3}$$

$$B_y(z,t) = \sqrt{\frac{2\omega^2}{V\varepsilon_0}} \frac{\mu_0 \varepsilon_0}{k} \dot{q}(t) \cos(kz). \tag{1.4}$$

Here we assumed periodic boundary conditions in an effective volume V with frequencies $\omega_m = c\frac{m\pi}{L}$ where $L^3 = V$. The terms $q(t)$ and $\dot{q}(t)$ describe position and momentum respectively. Note that $\ddot{q}(t) = -\omega^2 q(t)$.

The Hamiltonian of the EM-field is given as

$$\begin{aligned} H &= \frac{1}{2} \int \mathrm{d}V \, (\varepsilon_0 \boldsymbol{E}^2(\boldsymbol{r},t) + \frac{1}{\mu_0} \boldsymbol{B}^2(\boldsymbol{r},t)) \\ &= \frac{1}{2} \int \mathrm{d}V \, (\varepsilon_0 E_x^2(z,t) + \frac{1}{\mu_0} B_y^2(z,t)) = \frac{1}{2}(p^2 + \omega^2 q^2). \end{aligned} \tag{1.5}$$

Using the correspondence principle of quantum mechanics we can promote the variables q, p to operators $\hat{q}, \hat{p}$ and write the Hamiltonian as

$$\hat{H} = \frac{1}{2}(\hat{p}^2 + \omega^2 \hat{q}^2). \tag{1.6}$$

For our description we define a different set of variables, the ladder operators $\hat{a}$ and $\hat{a}^\dagger$

$$\hat{E}_x(z,t) = E_0(\hat{a} + \hat{a}^\dagger) \sin(kz) \quad E_0 \sim \sqrt{\frac{\hbar\omega}{\varepsilon_0 V}} \tag{1.7}$$

$$\hat{B}_y(z,t) = -\mathrm{i} B_0(\hat{a} - \hat{a}^\dagger) \cos(kz) \quad B_0 \sim \frac{\mu_0}{2} \sqrt{\frac{\varepsilon_0 \hbar \omega^3}{V}}. \tag{1.8}$$

Then we can rewrite the Hamiltonian as

$$\hat{H} = \hbar\omega \left(\hat{a}^\dagger \hat{a} + \frac{1}{2} \right). \tag{1.9}$$

Furthermore we want to state some properties of the ladder operators

$$[\hat{a}, \hat{a}^\dagger] = 1, \quad [\hat{a}, \hat{a}] = 0 = [\hat{a}^\dagger, \hat{a}^\dagger]. \tag{1.10}$$

Their time evolution is given by the HEISENBERG equation of motion

$$\begin{aligned}\frac{\mathrm{d}\hat{a}}{\mathrm{d}t} &= \frac{\mathrm{i}}{\hbar}[\hat{H},\hat{a}] = \mathrm{i}\left[\omega\left(\hat{a}^\dagger\hat{a}+\frac{1}{2}\right),\hat{a}\right] = \mathrm{i}\omega(\hat{a}^\dagger\hat{a}\hat{a}-\hat{a}\hat{a}^\dagger\hat{a}) \\ &= \mathrm{i}\omega\underbrace{[\hat{a}^\dagger,\hat{a}]}_{-1}\hat{a} = -\mathrm{i}\omega\hat{a}. \end{aligned} \tag{1.11}$$

Considering the SCHRÖDINGER equation we now want to find eigenstates and -values of the Hamiltonian. The eigenstates are called *photon number states* or *Fock states* $|n\rangle$. The eigenvalues are then

$$\begin{aligned}&\hat{H}|n\rangle = \hbar\omega\left(\hat{a}^\dagger\hat{a}+\frac{1}{2}\right)|n\rangle = E_n|n\rangle \\ &\Rightarrow E_n = \hbar\omega\left(n+\frac{1}{2}\right) \quad \text{with} \quad n=0,1,2,\ldots \end{aligned} \tag{1.12}$$

The state $|0\rangle$ with $n=0$ is called *vacuum* state. We can show that the action of the ladder operators on Fock states is given as

$$\begin{aligned}\hat{a}^\dagger|n\rangle &= \sqrt{n+1}\,|n+1\rangle \\ \hat{a}|n\rangle &= \sqrt{n}\,|n-1\rangle\,. \end{aligned} \tag{1.13}$$

We also want to state that the photon number state are orthogonal $\langle n|m\rangle = \delta_{mn}$.

If we consider a multi-mode regime the action of the ladder operator $\hat{a}_m^\dagger$ of the m-th optical mode is

$$\hat{a}_m^\dagger|0\rangle = \hat{a}_m^\dagger|0_1,0_2,\ldots,0_m,\ldots\rangle = |0_1,0_2,\ldots,1_m,\ldots\rangle = |1\rangle_m\,. \tag{1.14}$$

For example in a beam splitter with two input modes if we assume that one photon is in spatial mode one, then

$$|\mathrm{in}\rangle = \hat{a}_1^\dagger|0\rangle = |1\rangle_1\,. \tag{1.15}$$

1.2 Quantum fluctuations

Fock states $|n\rangle$ are states with a well defined number of photons/energy, but *not* well defined EM-field. The expectation value of the electric field is

$$\left\langle\hat{E}_x(z,t)\right\rangle = \left\langle n|\hat{E}_x(z,t)|n\right\rangle = E_0\sin(kz)\left\langle n|\hat{a}+\hat{a}^\dagger|n\right\rangle = 0. \tag{1.16}$$

We observe that the mean value of the electric field for $|n\rangle$ is zero. However, the mean value of the squared electric field is not

$$\begin{aligned}\left\langle\hat{E}_x^2(z,t)\right\rangle &= E_0^2\sin^2(kz)\left\langle n|(\hat{a}+\hat{a}^\dagger)^2|n\right\rangle \\ &= E_0^2\sin^2(kz)\left\langle n|\hat{a}^2+\underbrace{\hat{a}\hat{a}^\dagger}_{\to n+1}+\underbrace{\hat{a}^\dagger\hat{a}}_{\to n}+\hat{a}^{\dagger 2}|n\right\rangle \\ &= 2E_0^2\sin^2(kz)\left(n+\frac{1}{2}\right). \end{aligned} \tag{1.17}$$

Then we can calculate the field fluctuations as

$$\Delta\hat{E}_x = \sqrt{\langle \hat{E}_x^2 \rangle - \langle E_x \rangle^2} = \sqrt{2} E_0 \sin(kz) \sqrt{n + \frac{1}{2}}. \tag{1.18}$$

Its noteworthy that even for $n = 0$ the fluctuations $\Delta\hat{E}_x$ are nonzero. This effect is called *vacuum fluctuations*.

2 The generation of photon pairs

First we want to define the term of a photon pair. We define a photon pair as a Fock state of the following form

$$|\psi\rangle = \hat{a}_1^\dagger \hat{a}_2^\dagger |0\rangle \quad \text{with} \quad \langle \psi | \hat{N} | \psi \rangle = 2. \tag{2.1}$$

2.1 Time evolution, pictures, perturbation theory

First let us refresh on several concepts on quantum mechanics. In Quantum optics we use *states* to describe systems and *operators* to describe interactions. Up to now, the HEISENBERG picture was used. Here the time dependence is in the operators and states are time independent. Then the operators fulfill the HEISENBERG equation of motion

$$\frac{\mathrm{d}}{\mathrm{d}t} \hat{A}(t) = \frac{\mathrm{i}}{\hbar} [\hat{H}, \hat{A}(t)] + \frac{\partial \hat{A}}{\partial t}. \tag{2.2}$$

The time dependent operator is represented by

$$\hat{A}(t) = \hat{U}^\dagger(t) \hat{A}(t=0) \hat{U}(t), \tag{2.3}$$

where $\hat{U}(t) = \exp\left(-\frac{\mathrm{i}}{\hbar}\hat{H}t\right)$ is the time evolution operator. The expectation value of the operator $\hat{A}(t)$ is

$$\langle \hat{A}(t) \rangle = \langle \psi | \hat{A}(t) | \psi \rangle = \left\langle \psi | \hat{U}^\dagger(t) \hat{A}(t=0) \hat{U}(t) | \psi \right\rangle = \langle \psi(t) | \hat{A}(t=0) | \psi(t) \rangle. \tag{2.4}$$

Thus we can also define the states as time dependent and their evolution is governed by the SCHRÖDINGER equation

$$\mathrm{i}\hbar \frac{\partial}{\partial t} |\psi\rangle = \hat{H} |\psi\rangle \quad \Rightarrow \quad \text{formal solution:} \quad |\psi(t)\rangle = \underbrace{\exp\left(-\frac{\mathrm{i}}{\hbar}\hat{H}t\right)}_{\hat{U}(t)} |\psi(t=0)\rangle. \tag{2.5}$$

Thus this quantum mechanical picture is called SCHRÖDINGER picture. We now discuss the special case when the wave function is in an eigenstate of $\hat{H}$

$$\hat{H} |\psi(t)\rangle = E_n |\psi(t)\rangle \quad \Rightarrow \quad |\psi(t)\rangle = \exp\left(-\frac{\mathrm{i}}{\hbar} E_n t\right) |\psi(t=0)\rangle. \tag{2.6}$$

Finally we can also distribute the time evolution to states and operators respectively. This is called the DIRAC interaction picture. We consider a Hamiltonian in the SCHRÖDINGER picture

$$\hat{H}^{(S)} = \hat{H}_0^{(S)} + \hat{H}_{\text{int}}, \tag{2.7}$$

where $\hat{H}_0^{(s)}$ is the free Hamiltonian with known eigenstates and $\hat{H}_{\text{int}}$ is called interaction Hamiltonian, which is assumed to be a weak perturbation of the system.

The idea of the interaction picture is to separate the contributions of both Hamiltonians. The state is assumed to evolve according to the free Hamiltonian

$$\left|\psi^{(I)}(t)\right\rangle \equiv \hat{U}_0(t)\left|\psi^{(S)}(t=0)\right\rangle \quad \text{with} \quad \hat{U}_0(t) = \exp\left(-\frac{\mathrm{i}}{\hbar}\hat{H}_0^{(S)}\right), \tag{2.8}$$

where $\hat{U}_0(t)$ satisfies the time dependent SCHRÖDINGER equation. Since the expectation value of an operator $\hat{X}$ has to be identical in both pictures we have

$$\left\langle\psi^{(I)}(t)|\hat{X}^{(I)}(t)|\psi^{(I)}(t)\right\rangle = \left\langle\psi^{(S)}|\hat{U}_0\hat{X}^{(I)}(t)\hat{U}_0^\dagger|\psi^{(S)}\right\rangle \overset{!}{=} \left\langle\psi^{(S)}|\hat{X}^{(S)}|\psi^{(S)}\right\rangle \tag{2.9}$$

and find an expression for the operators in the interaction picture

$$\hat{X}^{(S)} = \hat{U}_0\hat{X}^{(I)}(t)\hat{U}_0^\dagger. \tag{2.10}$$

If we apply this to the free part of the Hamiltonian we see that $\hat{H}_0^{(I)} = \hat{H}_0^{(S)}$ because time evolution operator and Hamiltonian commute. Then the time evolution of the operators is given as

$$\mathrm{i}\hbar\frac{\partial\hat{X}^{(I)}(t)}{\partial t} = [\hat{X}^{(I)}(t), \hat{H}_0^{(S)}]. \tag{2.11}$$

We can see that the fast time evolution driven by the free Hamiltonian is carried by the operators while the time evolution of the interaction part is carried by the states

$$\mathrm{i}\hbar\frac{\partial}{\partial t}\left|\psi^{(I)}(t)\right\rangle = \hat{H}_{\text{int}}^{(I)}\left|\psi^{(I)}(t)\right\rangle. \tag{2.12}$$

The formal solution of this slow time evolution is given by

$$\left|\psi^{(I)}(t)\right\rangle = \hat{V}(t,t_0)\left|\psi^{(I)}(t_0)\right\rangle \quad \text{with} \quad \mathrm{i}\hbar\frac{\partial}{\partial t}\hat{V}(t,t_0) = \hat{H}^{(I)}(t)\hat{V}(t,t_0) \quad \text{and} \quad \hat{V}(t_0,t_0) = \mathbb{1}. \tag{2.13}$$

We can formally integrate this differential equation $\int \ldots \mathrm{d}t'$

$$\hat{V}(t,t_0) - \underbrace{\hat{V}(t_0,t_0)}_{\mathbb{1}} = \int_{t_0}^{t}\frac{\mathrm{d}}{\mathrm{d}t'}\hat{V}(t',t_0)\,\mathrm{d}t' = -\frac{\mathrm{i}}{\hbar}\int_{t_0}^{t}\hat{H}_{\text{int}}^{(I)}(t')\hat{V}(t',t_0)\,\mathrm{d}t \tag{2.14}$$

leading to the DYSON series

$$\hat{V}(t,t_0) = \mathbb{1} + \sum_{n=1}^{\infty} \left(-\frac{\mathrm{i}}{\hbar}\right)^n \int_{t_0}^{t} \mathrm{d}t_1 \ldots \int_{t_0}^{t_{n-1}} \mathrm{d}t_n \, \hat{H}_{\mathrm{int}}^{(I)}(t_1) \ldots \hat{H}_{\mathrm{int}}^{(I)}(t_n). \tag{2.15}$$

For small perturbations, the terms are getting smaller with increasing order. Then we can apply the first order perturbation and obtain

$$\hat{V}(t,t_0) \approx \mathbb{1} - \frac{\mathrm{i}}{\hbar} \int_{t_0}^{t} \mathrm{d}t_1 \, \hat{H}_{\mathrm{int}}^{(I)}(t_1). \tag{2.16}$$

The state in the SCHRÖDINGER picture is then given as

$$\left|\psi^{(S)}(t)\right\rangle = \hat{U}_0(t) \left[\mathbb{1} - \frac{\mathrm{i}}{\hbar} \int_{t_0}^{t} \mathrm{d}t_1 \, \hat{H}_{\mathrm{int}}^{(I)}(t_1)\right] \left|\psi^{(S)}(t_0)\right\rangle. \tag{2.17}$$

2.2 The SPDC interaction Hamiltonian

We now want to describe *spontaneous parametric down conversion* (SPDC) in a nonlinear medium. Here a pump photon can spontaneously split in a pair of signal and idler photons. We can describe this process using the polarization induced in a medium by the incoming electric field

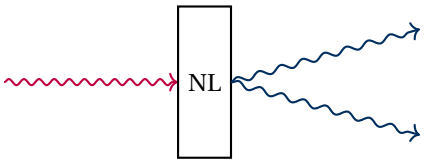

Fig. 1: SPDC process.

$$P_i = \underbrace{\varepsilon_0 \sum_j \chi_{ij}^{(1)} E_j}_{\text{linear optics } \chi^{(1)} \sim 1} \underbrace{+ \varepsilon_0 \sum_{j,k} \chi_{ijk}^{(2)} E_j E_k + \varepsilon_0 \sum_{j,k,l} E_j E_k E_l + \ldots}_{\text{NLO } \chi^{(2)} \sim 10^{-12} \frac{\mathrm{m}}{\mathrm{V}}} \tag{2.18}$$

In this expansion we assumed an instantaneously responsive, non-dispersive medium. For SPDC we concentrate on 2nd order effects

$$\hat{P}_i^{(2)} = \sum_{j,k} \chi_{ijk}^{(2)} \hat{E}_j \hat{E}_k. \tag{2.19}$$

The interaction Hamiltonian can then be written as

$$\hat{H}_{\mathrm{int}}(t) = \varepsilon_0 \int \mathrm{d}^3 r \, \hat{\boldsymbol{P}}^{(2)} \hat{\boldsymbol{E}} = \sum_{j,k,l} \varepsilon_0 \chi_{jkl}^{(2)} \int \mathrm{d}^3 r \, \hat{E}_{p,j} \hat{E}_{s,k} \hat{E}_{i,l}, \tag{2.20}$$

where the indices p, s, i stand for *pump, signal* and *idler* respectively. The fields can now be expanded in plane waves

$$\hat{E}_j(\boldsymbol{r},t) = \int \mathrm{d}^3 k \left[\hat{E}_j^{(-)} \mathrm{e}^{-\mathrm{i}(\omega t - \boldsymbol{k}\cdot\boldsymbol{r})} + \hat{E}_j^{(+)} \mathrm{e}^{+\mathrm{i}(\omega t - \boldsymbol{k}\cdot\boldsymbol{r})}\right] \quad \text{with} \tag{2.21}$$

$$\hat{E}_j^{(-)} = \mathrm{i}\sqrt{\frac{2\pi\hbar\omega}{V}} \hat{a}^\dagger(\boldsymbol{k}) \qquad \hat{E}_j^{(+)} = -\mathrm{i}\sqrt{\frac{2\pi\hbar\omega}{V}} \hat{a}(\boldsymbol{k}). \tag{2.22}$$

Substituting this back into equation (2.20) results in eight different combinations of annihilation/creation operators. For the SPDC process we only consider the case of creating a signal/idler photon, whereas the pump photon is annihilated. Since the pump is much stronger than signal/idler, we can treat it classically

$$\hat{E}_{p,j}(\boldsymbol{k}) \to E_{p,j}(k)\delta(\boldsymbol{k}-\boldsymbol{k}_p), \tag{2.23}$$

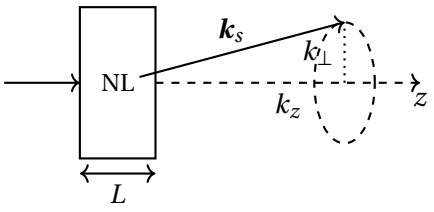

Fig. 2: Geometry of the wave vector.

meaning the pump is simply a plane wave. Now we can write down the interaction Hamiltonian as

$$\hat{H}_{\text{int}}(t) = C\int \mathrm{d}^3k_s\,\mathrm{d}^3k_i\,\mathrm{e}^{\mathrm{i}(\omega_p-\omega_s-\omega_i)t}\int_0^L \mathrm{d}z\,\mathrm{e}^{\mathrm{i}(k_{p_z}-k_{s_z}-k_{i_z})z}\int_A \mathrm{d}^2r_\perp\,\mathrm{e}^{\mathrm{i}(\boldsymbol{k}_{s\perp}+\boldsymbol{k}_{i\perp})\boldsymbol{r}_\perp}\hat{a}^\dagger(\boldsymbol{k}_s)\hat{a}^\dagger(\boldsymbol{k}_i), \tag{2.24}$$

where A is the surface of the NLO crystal and C contains all constants like E_p or $\chi^{(2)}_{ijk}$. For the transverse integral we can assume that A is much larger than the wavelength and can therefore assumed to be infinite

$$\int_A \mathrm{d}^2r_\perp\,\mathrm{e}^{\mathrm{i}(\boldsymbol{k}_{s\perp}+\boldsymbol{k}_{i\perp})\boldsymbol{r}_\perp} = 4\pi^2\delta^{(2)}(\boldsymbol{k}_{s\perp}+\boldsymbol{k}_{i\perp}) \quad\Rightarrow\quad \boldsymbol{k}_{s\perp} = -\boldsymbol{k}_{i\perp}. \tag{2.25}$$

This result corresponds to the physical expectation of conserved transverse momentum. For the longitudinal integral we introduce the phase mismatch $\Delta k = k_{p_z} - k_{s_z} - k_{i_z}$

$$\Phi(\Delta k\cdot L) = \frac{1}{L}\int_0^L \mathrm{d}z\,\mathrm{e}^{\mathrm{i}\Delta kz} = 2\mathrm{e}^{\mathrm{i}\Delta kL}\frac{\sin\left(\frac{\Delta kL}{2}\right)}{\Delta kL} = \mathrm{e}^{\mathrm{i}\Delta kL}\mathrm{sinc}\left(\frac{\Delta kL}{2}\right). \tag{2.26}$$

This corresponds to the phase matching condition, similar to classical nonlinear processes. Here, it is beneficial to have momentum conservation where $\boldsymbol{k}_s + \boldsymbol{k}_i = \boldsymbol{k}_p$.

Now the interaction Hamiltonian for SPDC becomes

$$\hat{H}_{\text{int}}(t) = C'\int \mathrm{d}^3k_s\,\mathrm{d}^3k_i\,\Phi(\Delta k\cdot L)\mathrm{e}^{\mathrm{i}(\omega_p-\omega_s-\omega_i)t}\delta^{(2)}(\boldsymbol{k}_{s\perp}+\boldsymbol{k}_{i\perp})\hat{a}^\dagger(\boldsymbol{k}_s)\hat{a}^\dagger(\boldsymbol{k}_i). \tag{2.27}$$

Now we try to calculate the two photon state using perturbation theory

$$|\psi\rangle = \exp\left(-\frac{\mathrm{i}}{\hbar}\int_{-T}^{T}\mathrm{d}t'\,\hat{H}_{\text{int}}t\right)|0\rangle \approx \left(\mathbb{1} - \frac{\mathrm{i}}{\hbar}\int_{-T}^{T}\mathrm{d}t'\,\hat{H}_{\text{int}} + \ldots\right)|0\rangle\,. \tag{2.28}$$

Since the interaction is small, a first order approximation is sufficient. The interaction time T can be considered infinite, since the nonlinearity is *instantaneous* and the time scale of NL interactions is much longer. The the time integral becomes

$$\int_{-\infty}^{\infty}\mathrm{d}t\,\mathrm{e}^{\mathrm{i}(\omega_p-\omega_s-\omega_i)t} = 2\pi\delta(\omega_p-\omega_s-\omega_i). \tag{2.29}$$

The delta function implies energy conservation with $\omega_p = \omega_s + \omega_i$. Now the state becomes

$$|\psi\rangle = -\frac{\mathrm{i}}{\hbar} C' \int \mathrm{d}^3 k_s \, \mathrm{d}^3 k_i \, \delta(\omega_p - \omega_s - \omega_i) \delta^{(2)}(\boldsymbol{k}_{s\perp} + \boldsymbol{k}_{i\perp}) \Phi(\Delta k \cdot L) \hat{a}^\dagger(\boldsymbol{k}_s) \hat{a}^\dagger(\boldsymbol{k}_i) |0\rangle . \tag{2.30}$$

The integral implicitly also runs over frequency, since the dispersion relation connects $\boldsymbol{k}$ and ω. The output state now contains two photons of signal and idler and contains the probability of generating them in specific modes governed by energy and momentum conservation.

2.3 Phase matching

For real nonlinear crystals phase matching is a problem due to dispersion. If we consider the simple, degenerate case of $\frac{\omega_p}{2} = \omega_s = \omega_i$, we then need $n_s = n_p$ for phase matching in forward direction.

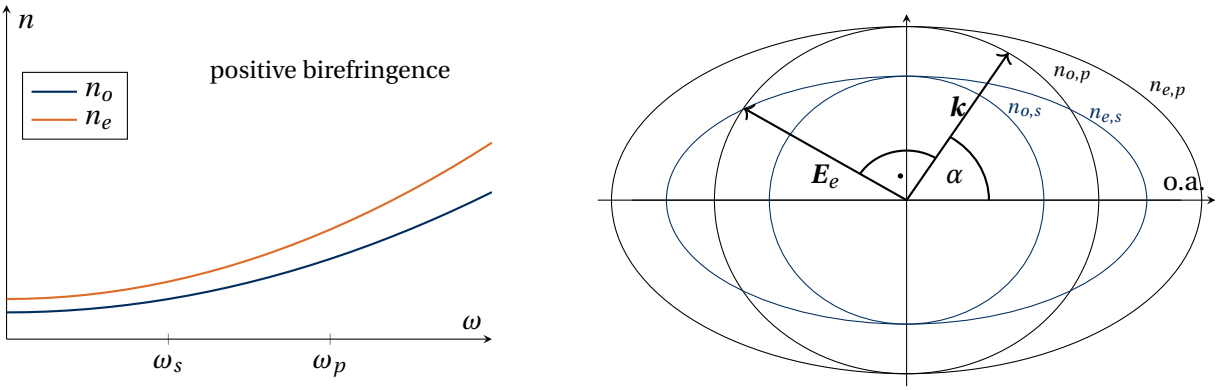

Fig. 3: Left: dispersion of ordinary and extraordinary axis of a nonlinear crystal.
Right: Index ellipsoid of the nonlinear crystal. If the propagation vector encloses the angle α with the optical axis (extraordinary index) ordinary index of the pump (black) and extraordinary index of the signal (blue) are matched.

The standard way to overcome this problem is to use a birefringent crystal. Typically we use uni-axial crystals where we have an ordinary axis with n_o for polarizations E_x, E_y and an extraordinary axis with n_e for polarizations E_z. For polarizations along x- and z-direction this can enable phase matching for specific frequencies (c. f. figure 3). We can see that phase matching can be achieved for different frequency combinations when different propagation directions are used. Typically we distinguish between two different types of phase matching:

- Type I: signal and idler same polarization, different for pump
- Type II: signal and idler different polarization

3 Fundamentals of quantum coherence

For the following discussions we want to focus on the effect of optical coherence in the quantized treatment of radiation.

3.1 First order coherence

3.1.1 Classical description

Classically we start with YOUNG's double slit experiment where we can produce interference fringes on a screen in the near field behind the double slit. We observe that interference fringes are only visible on the screen if the path difference Δs to the detector is smaller than the coherence length given by the bandwidth of the source $\Delta\omega$

$$\Delta s = |s_1 - s_2| \leq s_{\text{coh}} = \frac{c}{\Delta\omega}. \tag{3.1}$$

Hence, we can define a coherence time as $\Delta t_{\text{coh}} = \frac{\Delta s_{\text{coh}}}{c} = \frac{1}{\Delta\omega}$. The field on the detector at time t can be written as a linear superposition of the fields at earlier times

$$t_1 = t - \frac{s_1}{c} \quad \text{and} \quad t_2 = t - \frac{s_2}{c}. \tag{3.2}$$

The total electric field at the slits is the given by

$$\boldsymbol{E}(\boldsymbol{r}, t) = k_1 E(\boldsymbol{r}_1, t_1) + k_2 E(\boldsymbol{r}_2, t_2), \tag{3.3}$$

where $k_1, k_2 \in \mathbb{C}$ account for phases $\theta_{1,2}$ and limited slit transmission. Since the response

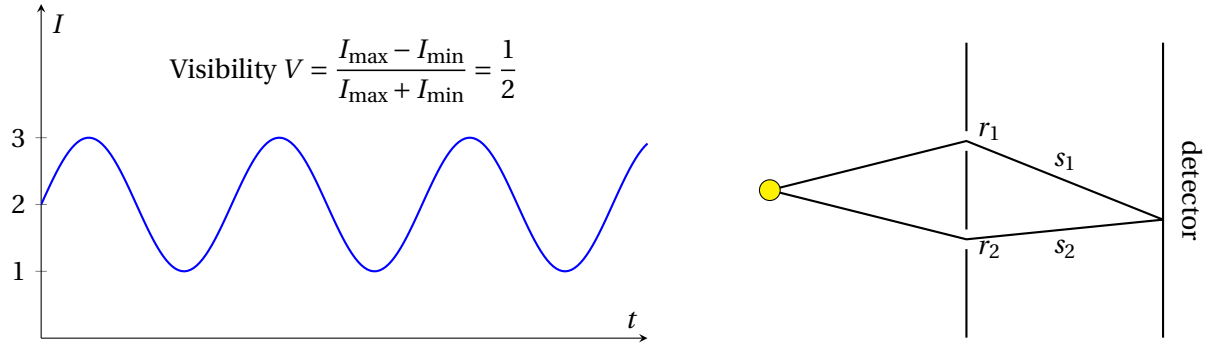

Fig. 4: Left: Temporal evolution of intensity for a visibility of 1/2.
Right: Double slit experiment.

time of the detector is long compared to the field oscillations the detector always averages over time. Thus we just measure the intensity

$$\begin{aligned} I(\boldsymbol{r}) &= \left\langle |E(\boldsymbol{r}, t)|^2 \right\rangle \\ &= |k_1|^2 \left\langle |E(\boldsymbol{r}_1, t_1)|^2 \right\rangle + |k_2|^2 \left\langle |E(\boldsymbol{r}_2, t_2)|^2 \right\rangle + 2\,\mathrm{Re}\left[k_1^* k_2 \left\langle E^*(\boldsymbol{r}_1, t_1) E(\boldsymbol{r}_2, t_2) \right\rangle \right] \\ &= I_1 + I_2 + 2\sqrt{I_1 I_2}\,\mathrm{Re}\left[k_1^* k_2 \frac{\langle E^*(\boldsymbol{r}_1, t_1) E(\boldsymbol{r}_2, t_2) \rangle}{\sqrt{I_1 I_2}} \right]. \end{aligned} \tag{3.4}$$

If we assume identical slits with a transmission of one we have $k_{12} = e^{i\theta_{12}}$

$$I(\boldsymbol{r}) = I_1 + I_2 + 2\sqrt{I_1 I_2}\underbrace{\mathrm{Re}\left[\frac{\langle E^*(\boldsymbol{r}_1,t_1)E(\boldsymbol{r}_2,t_2)\rangle}{\sqrt{I_1 I_2}}\right]}_{\text{interference contrast}}\cos(\theta_2-\theta_1). \tag{3.5}$$

The interference term leads us directly to the normalized classical first order *coherence* or *correlation* function

First order coherence function

$$\gamma^{(1)}(\boldsymbol{r}_1,t_1,\boldsymbol{r}_2,t_2) = \frac{\langle E^*(\boldsymbol{r}_1,t_1)E(\boldsymbol{r}_2,t_2)\rangle}{\sqrt{\left\langle|E(\boldsymbol{r}_1,t_1)|^2\right\rangle\left\langle|E(\boldsymbol{r}_2,t_2)|^2\right\rangle}} = \frac{\langle E^*(\boldsymbol{r}_1,t_1)E(\boldsymbol{r}_2,t_2)\rangle}{\sqrt{I_1\cdot I_2}} = |\gamma^{(1)}|e^{i\varphi_{12}}. \tag{3.6}$$

We can now classify the degree of coherence in the following way:

$$\begin{aligned} |\gamma^{(1)}| &= 1 && \text{fully coherent} \\ 0 < |\gamma^{(1)}| &< 1 && \text{partially coherent} \\ |\gamma^{(1)}| &= 0 && \text{incoherent.} \end{aligned} \tag{3.7}$$

Note that if the numerator factorizes

$$\left\langle E^*(\boldsymbol{r}_1,t_1)E(\boldsymbol{r}_2,t_2)\right\rangle = \left\langle E^*(\boldsymbol{r}_1,t_1)\right\rangle\langle E(\boldsymbol{r}_2,t_2)\rangle \quad \Rightarrow |\gamma^{(1)}| = 1. \tag{3.8}$$

This holds true for the quantum domain as well.

Temporal coherence

We now consider a monochromatic light field at fixed spatial positions at times t and $t+\tau$ propagating in z-direction with the electric field amplitude

$$E(z,t) = E_0 e^{i(kz-\omega t)} \quad \Rightarrow \quad E(z,t+\tau) = E_0 e^{i(kz-\omega(t+\tau))}. \tag{3.9}$$

For the first order correlation function we find

$$\begin{aligned} \gamma^{(1)}(z,t,t+\tau) = \gamma^{(1)}(\tau) &= \frac{\langle E^*(z,t)E(z,t+\tau)\rangle}{\sqrt{\langle|E(z,t)|\rangle^2}} = \ldots = e^{-i\omega\tau} \\ \Rightarrow |\gamma^{(1)}(\tau)|^2 &= 1. \end{aligned} \tag{3.10}$$

As expected, the monochromatic field is fully coherent since its coherence time $t_{\mathrm{coh}} = \frac{1}{\Delta\omega}$ is infinite.

3.1.2 Quantum description

From our quantum optics lecture we recall that

$$\begin{aligned}\hat{E}(\boldsymbol{r},t) &= \underbrace{\sqrt{\frac{\hbar\omega}{2\varepsilon_0 V}}}_{:=K}\left(\hat{a}\mathrm{e}^{\mathrm{i}(\boldsymbol{k}\cdot\boldsymbol{r}-\omega t)} - \hat{a}^\dagger \mathrm{e}^{-\mathrm{i}(\boldsymbol{k}\cdot\boldsymbol{r}-\omega t)}\right)\\ &= K\Big(\underbrace{\hat{a}\mathrm{e}^{\mathrm{i}\boldsymbol{k}\cdot\boldsymbol{r}}\mathrm{e}^{-\mathrm{i}\omega t}}_{\hat{E}^{(+)}(\boldsymbol{r},t)} - \underbrace{\hat{a}^\dagger \mathrm{e}^{-\mathrm{i}\boldsymbol{k}\cdot\boldsymbol{r}}\mathrm{e}^{\mathrm{i}\omega t}}_{\hat{E}^{(-)}(\boldsymbol{r},t)}\Big).\end{aligned} \tag{3.11}$$

Again we consider the double slit scenario and the superposition of the fields

$$\hat{E}^{(+)}(\boldsymbol{r},t) = K_1\hat{E}^{(+)}(\boldsymbol{r}_1,t_1) + K_2\hat{E}^{(+)}(\boldsymbol{r}_2,t_2). \tag{3.12}$$

Hence the intensity at the detector is

$$\begin{aligned}I(\boldsymbol{r},t) &= \left\langle \hat{E}^{(-)}(\boldsymbol{r},t)\hat{E}^{(+)}(\boldsymbol{r},t)\right\rangle =: G^{(1)}(\boldsymbol{r},t,\boldsymbol{r},t)\\ &= |K_1|^2\left\langle \hat{E}^{(-)}(\boldsymbol{r}_1,t_1)\hat{E}^{(+)}(\boldsymbol{r}_1,t_1)\right\rangle \qquad \to |K_1|^2 G^{(1)}(\boldsymbol{r}_1,t_1,\boldsymbol{r}_1,t_1) \quad \text{(slit 1)}\\ &+ |K_2|^2\left\langle \hat{E}^{(-)}(\boldsymbol{r}_2,t_2)\hat{E}^{(+)}(\boldsymbol{r}_2,t_2)\right\rangle \qquad \to |K_1|^2 G^{(1)}(\boldsymbol{r}_2,t_2,\boldsymbol{r}_2,t_2) \quad \text{(slit 2)}\\ &+ 2\,\mathrm{Re}\Big[K_1^* K_2 \underbrace{\left\langle \hat{E}^{(-)}(\boldsymbol{r}_1,t_1)\hat{E}^{(+)}(\boldsymbol{r}_2,t_2)\right\rangle}_{=G^{(1)}(\boldsymbol{r}_1,t_1,\boldsymbol{r}_2,t_2)}\Big].\end{aligned} \tag{3.13}$$

A normalization leads us to the first order coherence function

Normalized first order coherence function

$$\begin{aligned}g^{(1)}(\boldsymbol{r}_1,t_1,\boldsymbol{r}_2,t_2) &= \frac{\left\langle \hat{E}^{(-)}(\boldsymbol{r}_1,t_1)\hat{E}^{(+)}(\boldsymbol{r}_2,t_2)\right\rangle}{\sqrt{\left\langle \hat{E}^{(-)}(\boldsymbol{r}_1,t_1)\hat{E}^{(+)}(\boldsymbol{r}_1,t_1)\right\rangle\left\langle \hat{E}^{(-)}(\boldsymbol{r}_2,t_2)\hat{E}^{(+)}(\boldsymbol{r}_2,t_2)\right\rangle}}\\ &= \frac{G^{(1)}(\boldsymbol{r}_1,t_1,\boldsymbol{r}_2,t_2)}{G^{(1)}(\boldsymbol{r}_1,t_1,\boldsymbol{r}_1,t_1)G^{(1)}(\boldsymbol{r}_2,t_2,\boldsymbol{r}_2,t_2)}.\end{aligned} \tag{3.14}$$

As in the classical description we distinguish between different degrees of coherence

$$\begin{aligned}|g^{(1)}(\boldsymbol{r}_1,t_1,\boldsymbol{r}_2,t_2)| &= 1 \qquad \text{fully coherent}\\ 0 < |g^{(1)}(\boldsymbol{r}_1,t_1,\boldsymbol{r}_2,t_2)| &< 1 \qquad \text{partially coherent}\\ |g^{(1)}(\boldsymbol{r}_1,t_1,\boldsymbol{r}_2,t_2)| &= 0 \qquad \text{incoherent.}\end{aligned} \tag{3.15}$$

Example:

We consider a single plane wave mode of a quantized field propagation with a wave vector $\boldsymbol{k}$ with a positive frequency part of the field operator as

$$\hat{E}^{(+)}(\boldsymbol{r},t) = K\hat{a}\mathrm{e}^{\mathrm{i}(\boldsymbol{k}\cdot\boldsymbol{r}-\omega t)}. \tag{3.16}$$

If the field is in a photon number state $|n\rangle$, then we have

$$\begin{aligned} G^{(1)}(\boldsymbol{r},t,\boldsymbol{r},t) &= \langle n|\hat{E}^{(-)}(\boldsymbol{r},t)\hat{E}^{(+)}(\boldsymbol{r},t)|n\rangle = |K|^2\left\langle n|\hat{a}^\dagger\hat{a}|n\right\rangle = |K|^2 n. \\ G^{(1)}(\boldsymbol{r}_1,t_1,\boldsymbol{r}_2,t_2) &= \langle n|\hat{E}^{(-)}(\boldsymbol{r}_1,t_1)\hat{E}^{(+)}(\boldsymbol{r}_2,t_2)|n\rangle = |K|^2 n\mathrm{e}^{\mathrm{i}[\boldsymbol{k}(\boldsymbol{r}_2-\boldsymbol{r}_1)-(\omega_2-\omega_1)t]}. \end{aligned} \tag{3.17}$$

From that we can conclude

$$|g^{(1)}(\boldsymbol{r}_1,t_1,\boldsymbol{r}_2,t_2)| = 1 \quad \Rightarrow \quad \text{fully coherent.} \tag{3.18}$$

Furthermore we can also show that for a field in a coherent state $|\alpha\rangle$

$$|\alpha\rangle = \exp\left(-\frac{|\alpha|^2}{2}\right)\sum_{n=0}^{\infty}\frac{\alpha^n}{\sqrt{n!}}|n\rangle\,, \tag{3.19}$$

the first order coherence function $|g^{(1)}(\boldsymbol{r}_1,t_1,\boldsymbol{r}_2,t_2)| = 1$. Remarkably, all higher coherence functions of the coherent state are unity aswell.

Temporal coherence

We now want to consider the example of thermal light

$$\hat{E}^{(+)}(t) = E_0\mathrm{e}^{\mathrm{i}\omega t}\mathrm{e}^{\mathrm{i}\varphi(t)}\hat{a}, \tag{3.20}$$

where $\varphi(t)$ is a randomly varying phase. Then the temporal coherence function is

$$G^{(1)}(\tau) = \mathrm{e}^{\mathrm{i}\omega\tau}\underbrace{\left\langle\mathrm{e}^{\mathrm{i}(\varphi(t+\tau)-\varphi(t))}\right\rangle}_{\text{slowly varying envelope}}. \tag{3.21}$$

The shape of the envelope is connected to the dynamics in the source. Generally we distinguish two types of mechanisms

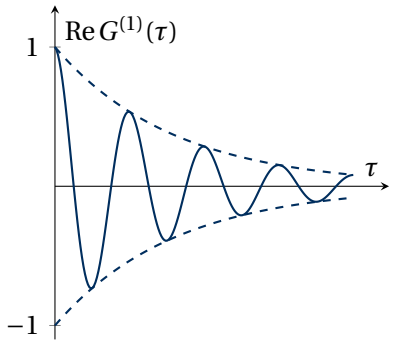

Fig. 5: Coherence function of thermal light.

- Source dominated by collisions of atoms (homogeneous broadening). Here we have a Lorentzian shaped spectrum. Thus the coherence function is (connected via Fourier transform)

$$G^{(1)}(\tau) = \mathrm{e}^{-\mathrm{i}\omega\tau}\mathrm{e}^{-\frac{\tau}{\tau_c}} \quad \text{with coherence time} \quad \tau_c = \frac{1}{\Delta\omega}. \tag{3.22}$$

- Source dominated by Doppler broadening (inhomogeneous). This results in a Gaussian shaped spectrum. Therefore the coherence function is

$$G^{(1)}(\tau) = \mathrm{e}^{-\mathrm{i}\omega\tau}\mathrm{e}^{-\frac{\pi}{2}\left(\frac{\tau}{\tau_c}\right)^2} \quad \text{with} \quad \tau_c = \frac{\sqrt{8\pi\ln 2}}{\Delta\omega}. \tag{3.23}$$

Note that the coherence time (as in the classical case) is inversely proportional to the bandwidth $\Delta\omega$ of the light source. We obtained the results for the coherence functions using the WIENER-KHINCHINE theorem which connects the temporal first order correlation function and the spectral intensity distribution $F(\omega)$ of the light source

$$F(\omega) = \frac{1}{2\pi}\int_{-\infty}^{\infty} g^{(1)}(\tau)\mathrm{e}^{-\mathrm{i}\omega\tau}\,\mathrm{d}\tau\,. \tag{3.24}$$

3.2 Second-order quantum coherence function

3.2.1 Classical description

The first order coherence function does not contain information about the statistical properties of light. Instead, we can perform intensity correlations as in the *Hanbury Brown-Twiss experiment*. This experiment (schematically drawn in figure 6) is measuring correlations between the intensity fluctuations of light a different times. The detectors may be single photon detectors giving us the coincidence rate between the two detectors or normal photo diodes where we measure the signal correlation for varying time delay τ. Since the intensity is the same for both arms the coincidence rate is

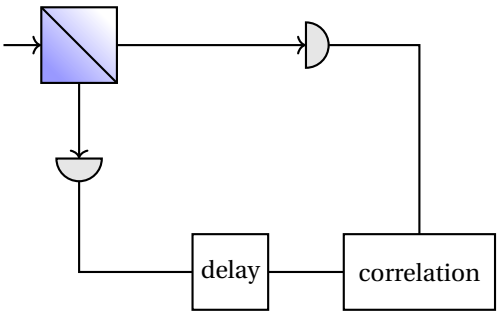

Fig. 6: Hanbury Brown-Twiss experiment.

$$c(t, t+\tau) = \langle I(t) I(t+\tau) \rangle , \tag{3.25}$$

and thus we can write the normalized second-order coherence function as

Normalized Second order coherence function

$$\gamma^{(2)}(\tau) = \frac{\langle I(t) I(t+\tau) \rangle}{\langle I(t) \rangle^2} = \frac{\langle E^*(t) E^*(t+\tau) E(t+\tau) E(t) \rangle}{\langle E^*(t) E(t) \rangle^2}. \tag{3.26}$$

We can write this for spatial coordinates in the same way. A light field is called second-order coherent, when $|\gamma^{(1)}(\tau)| = 1$ and $|\gamma^{(2)}(\tau)| = 1$.

Example: Monochromatic plane wave

In the special case of a monochromatic plane wave $E(z,t) = E_0 \mathrm{e}^{\mathrm{i}(kz-\omega t)}$ we find $\gamma^{(1)}(\tau) = \mathrm{e}^{-\mathrm{i}\omega\tau}$ and thus $|\gamma^{(1)}| = 1$. The second-order coherence also gives

$$\gamma^{(2)}(\tau) = \frac{|E_0|^4}{\langle E^*(t) E(t) \rangle^2} = 1 \quad \Rightarrow \quad \text{2nd order coherent.} \tag{3.27}$$

In fact, any field with constant intensity will have $\gamma^{(2)}(\tau) = 1$.

Boundaries of the correlation values

Now we might wonder what are possible values of $\gamma^{(2)}$. Let us consider first $\tau = 0$

$$\gamma^{(2)}(0) = \frac{\langle I^2(t) \rangle}{\langle I(t) \rangle^2}. \tag{3.28}$$

The average values of the intensity are determined by N measurements at different absolute times

$$\langle I(t)\rangle = \frac{I(t_1)+\ldots+I(t_N)}{N}, \quad \left\langle I^2(t)\right\rangle = \frac{I^2(t_1)+\ldots+I^2(t_N)}{N}. \tag{3.29}$$

For $N=2$ we can make use of the CAUCHY-SCHWARTZ inequality $2I_1I_2 \le I_1^2+I_2^2$ for any real numbers I_1, I_2

$$(I_1+I_2)^2 = I_1^2+I_2^2+2I_1I_2 \le 2(I_1^2+I_2^2). \tag{3.30}$$

We can generalize this to N intensities

$$\langle I(t)\rangle^2 = \frac{1}{N^2}(I_1+\ldots+I_N)^2 \le \frac{1}{N}(I_1^2+\ldots+I_N^2) = \left\langle I^2(t)\right\rangle. \tag{3.31}$$

Thus we find

$$1 \le \gamma^{(2)}(0) < \infty. \tag{3.32}$$

We do not have an upper bound for $\gamma^{(2)}(0)$, however, its minimum value is one. We can also derive that

$$\langle I(t)I(t+\tau)\rangle \le \left\langle I^2(t)\right\rangle \quad \Rightarrow \quad \gamma^{(2)}(\tau) \le \gamma^{(2)}(0). \tag{3.33}$$

The probability of detecting coincidences is highest for zero delay. This leads us to the terminology of *photon bunching*.

Example: Thermal light

One can show that for thermal light the second and first order coherence functions are related via the SIEGERT relation, i. e.

$$\gamma^{(2)}(\tau) = 1+|\gamma^{(1)}(\tau)|^2. \tag{3.34}$$

For a collision broadened source (c. f. figure 7) we find

$$\gamma^{(2)}(\tau) = 1+\exp\left(-2\frac{|\tau|}{\tau_c}\right). \tag{3.35}$$

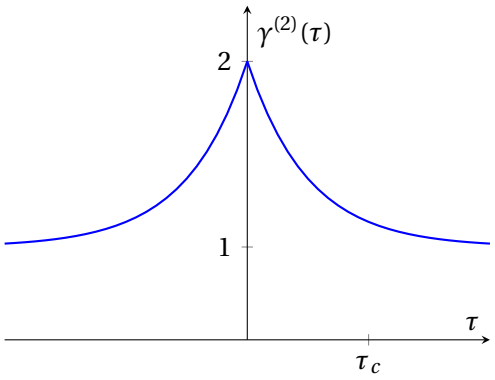

Fig. 7: 2nd order coherence function of a thermal light source.

3.2.2 Quantum description

Performing again the transition toward the quantum domain we obtain for the second order coherence function

Normalized Second order coherence function

$$\gamma^{(2)}(\tau) = \frac{\left\langle \hat{E}^{(-)}(t)\hat{E}^{(-)}(t+\tau)\hat{E}^{(+)}(t+\tau)\hat{E}^{(+)}(t)\right\rangle}{\left\langle \hat{E}^{(-)}(t)\hat{E}^{(+)}(t)\right\rangle\left\langle \hat{E}^{(-)}(t+\tau)\hat{E}^{(+)}(t+\tau)\right\rangle}. \tag{3.36}$$

In the following we want to discuss several examples of second order coherence functions:

- *Single mode field*: $\hat{E}^{(+)} = \mathrm{i}K\hat{a}\mathrm{e}^{\mathrm{i}(\boldsymbol{k}\cdot\boldsymbol{r}-\omega t)}$

$$\Rightarrow g^{(2)}(\tau) = \frac{\left\langle \hat{a}^\dagger \hat{a}^\dagger \hat{a}\hat{a} \right\rangle}{\left\langle \hat{a}^\dagger \hat{a} \right\rangle^2} = \frac{\langle \hat{n}(\hat{n}-1) \rangle}{\langle \hat{n} \rangle^2} = 1 + \frac{\left\langle (\Delta\hat{n})^2 \right\rangle - \langle \hat{n} \rangle}{\langle \hat{n} \rangle^2}. \tag{3.37}$$

  We observe that for single-mode fields the 2nd order coherence function is independent on τ.

- *Coherent state*: $\left\langle (\Delta\hat{n})^2 \right\rangle = \langle \hat{n} \rangle$. For a coherent state the distribution of photon numbers follows a Poissonian distribution with the property that the mean photon value is identical to the fluctuations. The 2nd order coherence function is thus $g^{(2)}(\tau) = 1$ which corresponds to a classical harmonic wave. Therefore, coherent states are suited to describe monochromatic laser fields.

- *Thermal light*: Same result as discussed before $g^{(2)}(\tau) = \gamma^{(2)}(\tau) = 1 + \mathrm{e}^{-2\frac{\tau}{\tau_c}}$.
  Thermal light always shows classical behaviour with $g^{(2)}(0) \geq g^{(2)}(\tau)$.

- *Photon number state*: As the name suggest the photon fluctuation $(\Delta n)^2 = 0$. Therefore we find

$$g^{(2)}(\tau) = \begin{cases} 0 & n = 0 \\ 1 - \frac{1}{n} & n \geq 1. \end{cases} \tag{3.38}$$

  Hence, $g^{(2)}(0) < 1$ is possible, which is not allowed in the classical domain.

Note that $g^{(2)}(0) \leq g^{(2)}(\tau)$ corresponds to the non-classical effect of photon anti-bunching. Consider an excited atom spontaneously emitting a photon. This generated single photon number state has these non-classical properties. We can summarize our results to

$$g^{(2)}(\tau) = \begin{cases} > 1 & \text{super-Poissonian, photon bunching} \quad \Rightarrow \quad \text{thermal light} \\ = 1 & \text{Poissonian, random spacing} \quad \Rightarrow \quad \text{laser light} \\ < 1 & \text{sub-Poissonian, photon anti-bunching} \quad \Rightarrow \quad \text{non-classical light.} \end{cases} \tag{3.39}$$

Fluctuation correlations

We can also use the 2nd order correlation function to characterize fluctuation correlations. Assume $I(t) = \langle I \rangle + \Delta I(t)$ with $\langle \Delta I(t) \rangle = 0$. Then we have

$$g^{(2)}(\tau) = \frac{\langle I(t) I(t+\tau) \rangle}{\langle I(t) \rangle \langle I(t+\tau) \rangle} = \frac{\langle [\langle I \rangle + \Delta I(t)][\langle I \rangle + \Delta I(t+\tau)] \rangle}{\langle I(t) \rangle^2} = 1 + \frac{\langle \Delta I(t) \Delta I(t+\tau) \rangle}{\langle I(t) \rangle^2}. \tag{3.40}$$

This is a measure for the correlation between intensity (or photon number) fluctuation. This will lead later on to the method of *Ghost imaging*.

3.3 Beam splitters with non-classical light

In the following we consider a beam splitter with reflection coefficient r and transmission coefficient t with $r, t \in \mathbb{C}$ and $|r|^2 + |t|^2 = 1$. We *always* have to consider two input and output modes, for example a single photon entering port $1'$ is described by

$$|\text{in}\rangle = \hat{a}^\dagger_{1'}|0\rangle = |1\rangle_{1'}|0\rangle_{2'}. \tag{3.41}$$

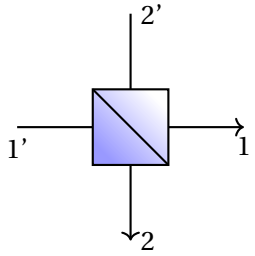

Fig. 8: Beam splitter setup.

The BS will split the possibilites to find the photon either in port 1 with probability $|t|^2$ or in port 2 with probability $|r|^2$. For a single photon state, no coincidences are possible. The beam splitter transformation looks as follows

$$\hat{a}^\dagger_{1'}|0\rangle \xrightarrow{\text{BS}} (t\hat{a}^\dagger_1 + r\hat{a}^\dagger_2)|0\rangle. \tag{3.42}$$

Analogously, for a photon in input port 2 we have

$$\hat{a}^\dagger_{2'}|0\rangle \xrightarrow{\text{BS}} (r\hat{a}^\dagger_1 + t\hat{a}^\dagger_2)|0\rangle. \tag{3.43}$$

This way we have a clear input to output correspondence. Often we relate the output to the input modes in a compact matrix formalism

$$\begin{pmatrix}\hat{a}^\dagger_1\\ \hat{a}^\dagger_2\end{pmatrix} = \begin{pmatrix}t & r\\ r & t\end{pmatrix}\begin{pmatrix}\hat{a}^\dagger_{1'}\\ \hat{a}^\dagger_{2'}\end{pmatrix}. \tag{3.44}$$

Typically most BS consist of a dielectric layer which results in a $\frac{\pi}{2}$ phase jump in case of reflection. We can now give some examples of BS acting on different input states:

- vacuum: $|0\rangle_{1'}|0\rangle_{2'} \xrightarrow{\text{BS}} |0\rangle_1|0\rangle_2$
- 50/50 BS: $\hat{a}^\dagger_{1'}|0\rangle \xrightarrow{\text{BS}} \frac{1}{\sqrt{2}}(\hat{a}^\dagger_1 + \mathrm{i}\hat{a}^\dagger_2)|0\rangle$
  Note that since we cannot factorize this state as a product of single mode states we call this a *path entangled state*.
- coherent state at a 50/50 BS in input port 1'. Here we introduce a *displacement operator* which creates a coherent state

$$\begin{aligned}|\alpha\rangle_{1'}|0\rangle_{2'} &= D(\alpha)|0\rangle_{1'}|0\rangle_{2'} = \exp\left(\alpha\hat{a}^\dagger_{1'} - \alpha^*\hat{a}_{1'}\right)|0\rangle_{1'}|0\rangle_{2'}\\ &\xrightarrow{\text{BS}} \exp\left(\frac{\alpha}{\sqrt{2}}[\hat{a}^\dagger_1 + \mathrm{i}\hat{a}^\dagger_2] - \frac{\alpha^*}{\sqrt{2}}[\hat{a}_1 - \mathrm{i}\hat{a}_2]\right)|0\rangle_1|0\rangle_2\\ &= \exp\left(\frac{\alpha}{\sqrt{2}}\hat{a}^\dagger_1 - \frac{\alpha^*}{\sqrt{2}}\hat{a}_1\right)\exp\left(\mathrm{i}\frac{\alpha}{\sqrt{2}}\hat{a}^\dagger_2 - \frac{-\mathrm{i}\alpha^*}{\sqrt{2}}\hat{a}_2\right)|0\rangle_1|0\rangle_2\\ &= \left|\frac{\alpha}{\sqrt{2}}\right\rangle_1\left|\frac{\mathrm{i}\alpha}{\sqrt{2}}\right\rangle_2. \end{aligned} \tag{3.45}$$

  Here the state is already factorized. We call this a *separable state*. The intensity is split equally to $\frac{|\alpha|^2}{2}$.

From the example of the coherent state we can see that a strongly attenuated laser source is *no* replacement for a single photon source.

Hong-Ou-Mandel effect

We now consider two indistinguishable photons, one in each input port of a 50/50 beam splitter

$$\begin{aligned}\hat{a}^\dagger_{1'}\hat{a}^\dagger_{2'}|0\rangle &= |1\rangle_{1'}|1\rangle_{2'} \\ &\Rightarrow \frac{1}{2}\left[(\hat{a}^\dagger_1 + \mathrm{i}\hat{a}^\dagger_2)(\mathrm{i}\hat{a}^\dagger_1 + \hat{a}^\dagger_2)\right]|0\rangle \\ &= \frac{1}{2}\left[\mathrm{i}(\hat{a}^\dagger_1)^2 + \mathrm{i}(\hat{a}^\dagger_2)^2 + \hat{a}^\dagger_1\hat{a}^\dagger_2 - \hat{a}^\dagger_1\hat{a}^\dagger_2\right]|0\rangle \\ &= \frac{\mathrm{i}}{2}\left[(\hat{a}^\dagger_1)^2 + (\hat{a}^\dagger_2)^2\right]|0\rangle = \frac{\mathrm{i}}{\sqrt{2}}(|2,0\rangle + |0,2\rangle). \end{aligned} \tag{3.46}$$

We again have a path-entangled two-photon state. Since both photons are always on the same output port we will not observe any coincidences between the output ports. This effect is called Hong-Ou-Mandel effect (HOM-effect). The schematic of the experiment carried out by Hong-Ou-Mandel[1] is shown in figure 9.

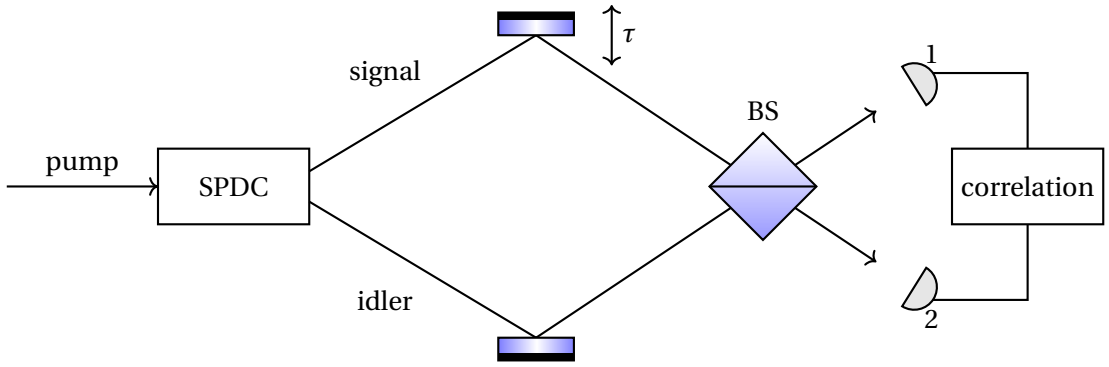

Fig. 9: Signal and idler photons produced by a type-I phase matching SPDC process in KDP are aligned to meet at a beam splitter. Spectral filtering ensures that only photon pairs with the same frequency are selected.

Here, a nonlinear crystal was used as a source of photon pairs where each photon was emitted in two different spatial modes. For a time delay $\tau = 0$ between both arms, the coincidence rate is zero due to the indistinguishability of the two photons. When the difference in arrival times gets larger, both photons become distinguishable and thus we can detect coincidences again. The minimum drops to zero only if the two photons are perfectly identical in all properties. The precise shape of the dip is directly related to the power spectrum of the single-photon wave packet and is therefore

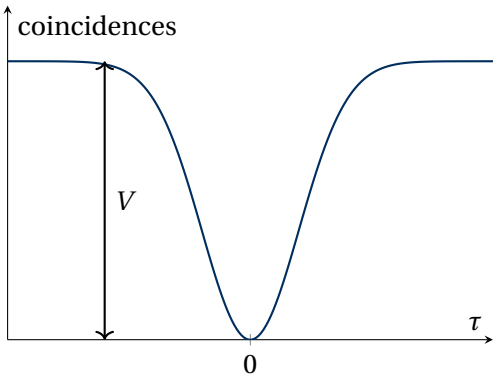

Fig. 10: Coincidence measurement.

[1] C. K. Hong, Z. Y. Ou and L. Mandel, Measurement of Subpicosecond Time Intervals between Two Photons by Interference, Phys. Rev. Lett. 59, 2044 (1987)

determined by the physical process of the source. According to Hong-Ou-Mandel the expected number N_c of observed photon coincidences is given by

$$N_c \sim R^2 + T^2 - 2RT \frac{\int_{-\infty}^{\infty} g(\tau)\, g(\tau - 2\delta\tau)\, \mathrm{d}\tau}{\int_{-\infty}^{\infty} g^{(2)}(\tau)\, \mathrm{d}\tau}. \tag{3.47}$$

We can also define a *visibility* for this experiment as

$$V = \frac{I_{\max} - I_{\min}}{I_{\max} + I_{\min}}, \tag{3.48}$$

which would be equal to one in the ideal case. In a real experiment we still have residual distinguishability due to the different wavelengths of signal and idler or a non-perfect beam splitter.

CAVE: The interference of the two-photon state happens at the detector and not the BS. Especially the interference does not depend on whether the photons overlap at the position of the beam splitter. We also want to emphasize that the two-photon interference is *not* the interference of two photons. It is the interference of one two-photon wave function with itself.

4 Applications of one- and two-photon interference

4.1 Interferometer with single photons

We now want to consider first a Mach-Zehnder interferometer setup with single photons. We assume a photon in spatial port $1''$. Then the action of the beam splitter 1, phase delay θ and beam splitter 2 can be calculated as

$$\begin{aligned}\hat{a}^\dagger_{1''}|0\rangle &\xrightarrow{\text{BS1}} \frac{1}{\sqrt{2}}(\hat{a}^\dagger_{1'} + \mathrm{i}\hat{a}^\dagger_{2'})|0\rangle \\ &\xrightarrow{\theta} \frac{1}{\sqrt{2}}(\hat{a}^\dagger_{1'} + \mathrm{i}\mathrm{e}^{\mathrm{i}\theta}\hat{a}^\dagger_{2'})|0\rangle \\ &\xrightarrow{\text{BS2}} \frac{1}{2}(\hat{a}^\dagger_1 + \mathrm{i}\hat{a}^\dagger_2 + \mathrm{i}\mathrm{e}^{\mathrm{i}\theta}\hat{a}^\dagger_2 - \mathrm{e}^{\mathrm{i}\theta}\hat{a}^\dagger_1)|0\rangle \\ &= \frac{1}{2}\left((1-\mathrm{e}^{\mathrm{i}\theta})\hat{a}^\dagger_1 + \mathrm{i}(1+\mathrm{e}^{\mathrm{i}\theta})\hat{a}^\dagger_2\right)|0\rangle\,. \end{aligned} \tag{4.1}$$

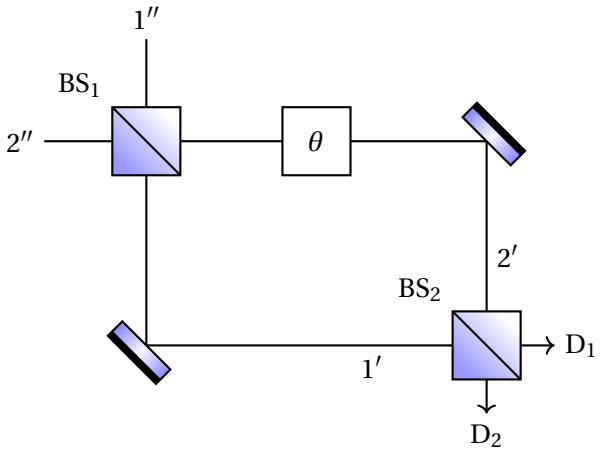

Fig. 11: Mach Zehnder interferometer setup.

Then the probability to find a photon in D_1 and D_2 is

$$P_{D_1} = \left|\frac{1}{2}(1-\mathrm{e}^{\mathrm{i}\theta})\right|^2 = \frac{1}{2}(1-\mathrm{e}^{\mathrm{i}\theta})(1-\mathrm{e}^{-\mathrm{i}\theta}) = \frac{1}{2}(1-\cos\theta) \tag{4.2}$$

$$P_{D_2} = \left|\frac{1}{2}(1+\mathrm{e}^{\mathrm{i}\theta})\right|^2 = \frac{1}{2}(1+\cos\theta). \tag{4.3}$$

We observe that we can change the signal on the detectors periodically by introducing a phase delay in one of the paths. The special case $\theta = 0$ of zero phase delay shows, that the photon will always hit detector two. This can be explained by the fact that the photon accumulates a phase shift of $\frac{\pi}{2}$ at every reflection. For the photon to hit detector one we have two paths, but their phase is shifted by π since along spatial mode $1'$ we have no reflection, whereas in spatial mode $2'$ the photon is reflected twice. The two one-photon probabilities then interfere destructively.

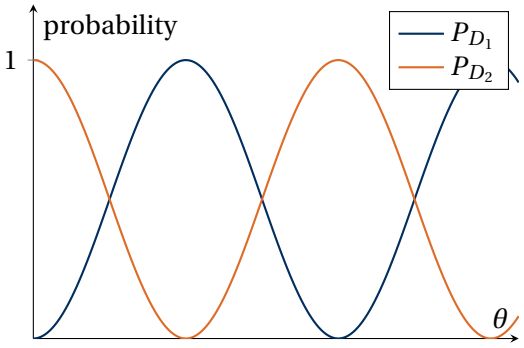

Fig. 12: Probability of photon detection.

Elitzur-Vaidman bomb test

We now want to use the single photon interferometer to raise the question, whether or not we might be able to obtain information about the presence of an object without interacting with it. That is the idea of *interaction free measurement*. We consider a set of bombs. Some of them are duds and are fully transparent to light, however, some are live and will detonate when absorbing even a single photon.

Now we place a bomb of our set into spatial port two of our interferometer. We may consider two different cases:

1. Bomb is a dud:
   The bomb is fully transparent, we have the case of no object. Only D_2 fill give a signal, whereas D_1 is dark.
2. bomb is live:
   - If the photon takes port 2 it will hit the bomb and thus we will have an explosion. This will fail our mission.
   - If the photon takes port 1 it will hit either D_1 or D_2 with 25 % each.

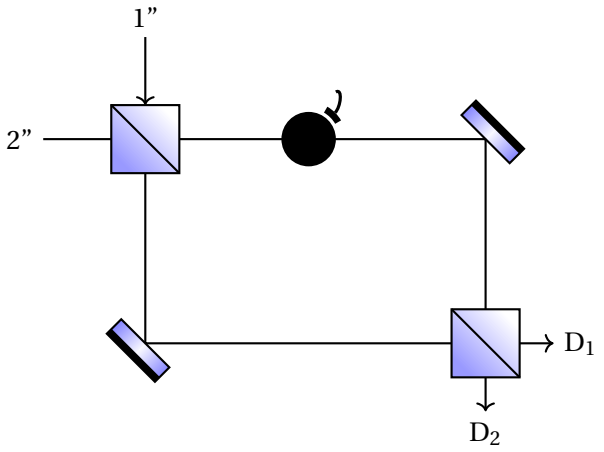

Fig. 13: Mach Zehnder interferometer setup.

Now, if we measure a photon in detector D_2, we will know for sure, that the bomb is live and did not explode. However, we will only succeed in our mission 25 % of the time. Thus we might wonder if we can increase the success rate?

For our experiment the actual success rate is higher than 25 % since we can repeat our measurement with another photon if the bomb did not explode before. We can only detect live bombs, therefore we assume a live bomb for now. In the first measurement we have a quarter chance of detecting the live bomb. If however, the photon took path 1 and the bomb did not explode (25 % chance as well) we can repeat the measurement and try again. So finally, for two 50/50 beam splitter we obtain

$$p = \sum_{n=1}^{\infty} \left(\frac{1}{4}\right)^n = \frac{1/4}{1-1/4} = \frac{1}{3}. \tag{4.4}$$

In general, the fraction η of measurements that can be interaction free is

$$\eta = \frac{p(\text{detection})}{p(\text{detection}) + p(\text{absorption})} = \frac{1/4}{1/4+1/2} = \frac{1}{3}. \tag{4.5}$$

Now we want to consider two beam splitters with different reflectivity and transmittance with $a \ll b$

$$\begin{aligned} &\text{BS1:} \quad |r| = a, \quad |t| = b \quad \Rightarrow \quad \text{mostly transparent} \\ &\text{BS1:} \quad |r| = b, \quad |t| = a \quad \Rightarrow \quad \text{mostly reflective} \quad . \end{aligned} \tag{4.6}$$

Now, in case of a dud only D_2 detects a photon and D_1 stays dark. If the bomb is live we will observe the following distributions:

$$P = a^2 \quad \text{explosion}, \quad P = a^2 b^2 \quad \text{success}, \quad P = b^4 \quad \text{hitting } D_2 \quad . \tag{4.7}$$

Then the fraction of interaction free measurements is

$$\eta = \frac{a^2 b^2}{a^2 b^2 + a^2} = \frac{b^2}{1+b^2} \xrightarrow{b^2 \to 1} \frac{1}{2}. \tag{4.8}$$

However, we can further improve our results by considering another setup (c. f. figure 14). Here we place a large bomb in the whole upper area of the setup. We model the reflectivity of the beam splitters in such a way that

$$|r|^2 = \cos^2\left(\frac{\pi}{2N}\right) \tag{4.9}$$

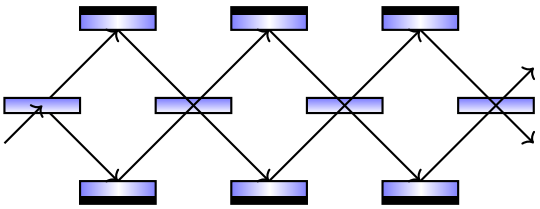

Fig. 14: Advanced interferometer setup.

for N beam splitters and $|r|^2+|t|^2 = 1$. Then the probability of successfully detecting a photon after N-beam splitters is

$$P_{\text{success}} = \left[\cos^2\left(\frac{\pi}{2N}\right)\right]^N \approx 1 - \frac{\pi^2}{4N} + \mathcal{O}\left(\frac{1}{N^2}\right). \tag{4.10}$$

The probability of absorption is just $1 - P_{\text{success}}$ and therefore

$$\eta = \frac{P_{\text{success}}}{P_{\text{success}} + P_{\text{absorb.}}} = P_{\text{success}} \approx 1 - \frac{\pi^2}{4N} \to 1 \quad \text{for} \quad N \to \infty. \tag{4.11}$$

Already for $N \geq 4$ we exceed the previous fraction of $\eta = \frac{1}{2}$.

4.2 Induced coherence and measurements with undetected light

Now we want to discuss an experiment performed by Zou, Wang and Mandel in 1991[2] and sketched in figure 15.

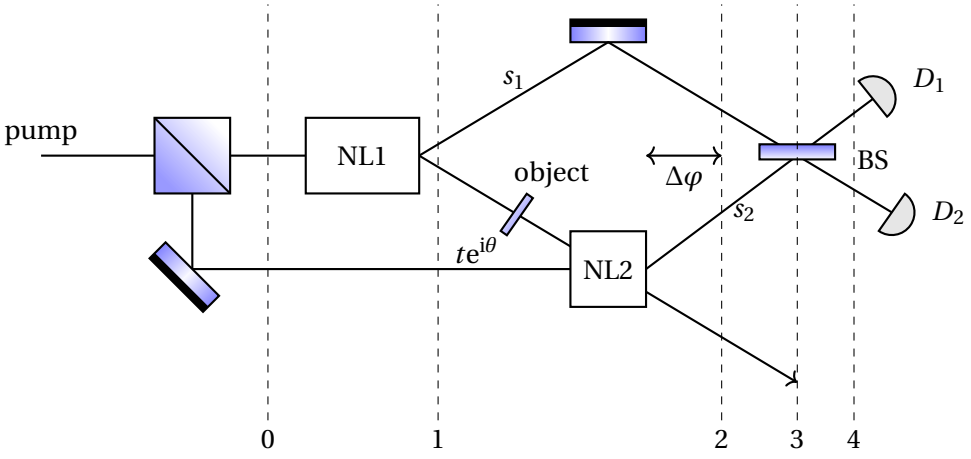

Fig. 15: Two similar nonlinear crystals NL are optically pumped by two mutually coherent pump waves, each emitting a signal and idler photon. We look for interference between the signal photons s_1 and s_2 whose trajectories meet at the beam splitter (BS). The trajectories of the two idlers i_1, i_2 are also aligned as shown.

This experiment demonstrated that interference effects take place if the paths of photons are indistinguishable, i. e. you cannot measure the "which-path" information.

[2] X. Y. Zou, L. J. Wang, and L. Mandel, "Induced coherence and indistinguishability in optical interference," Phys. Rev. Lett. 67, 318 (1991)

Since the output modes of the generated signal and idler photons overlap spatially, we cannot distinguish them. In this case we will observe interference in the count rates as shown by curve A in figure 16. If now an object is inserted (c. f. figure 15) in the beam path of the idler photons, the indistinguishability is lifted, as measuring the idler photons correlated with the signal photon could potentially provide information about the origin of the signal photons. Consequently the interference vanishes, as shown in curve B. Here, we do not actually obtain the "which-path" information, its sufficient that the information can in principle be obtained.

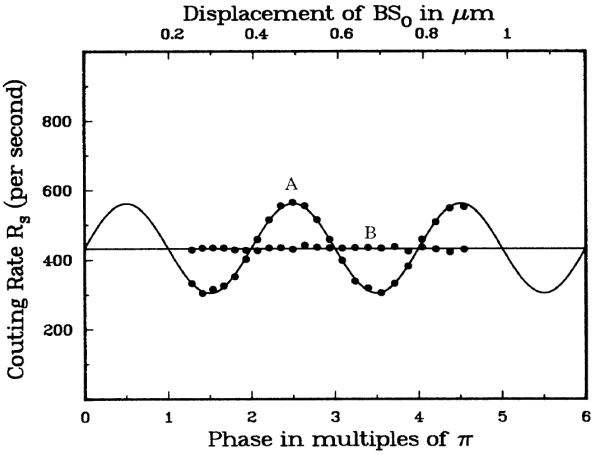

Fig. 16: Photon counting rate as function of beam splitter displacement.
Curve A: ND-filter with $|t| = 0.91$
Curve B: ND-filter with $|t| \approx 0$.

This phenomenon is interesting since signal and idler photons can have different wavelengths and measurements in wavelength ranges without any available detectors can be performed by only detecting (visible) signal photons.

In order to compare the experimental results with our developed theory of two-photon interference we want to perform the necessary calculations. At point "0" in figure 15 we have the following quantum state

$$|\text{in}\rangle = \frac{1}{\sqrt{2}}(\hat{a}^\dagger_{p_1} + \mathrm{i}\hat{a}^\dagger_{p_2})\,|0\rangle \tag{4.12}$$

$$\xrightarrow{1} \frac{1}{\sqrt{2}}(\alpha\,\hat{a}^\dagger_{s_1}\hat{a}^\dagger_{i_1} + \mathrm{i}\hat{a}^\dagger_{p_2})\,|0\rangle\,. \tag{4.13}$$

The factor α accounts for a not fully converted pump in NL1. We neglect the part $(1-\alpha)\hat{a}^\dagger_p$ since its irrelevant for our experiment (just place a spectral filter to filter out the pump radiation). Then we consider the transformation of the idler path due to the object

$$\hat{a}^\dagger_{i_1} \longrightarrow t\mathrm{e}^{\mathrm{i}\theta}\hat{a}^\dagger_{i_1} + \underbrace{\mathrm{i}\sqrt{1-|t|^2}\hat{a}^\dagger_{\text{loss}}}_{\text{loss modes}}. \tag{4.14}$$

the collective loss modes will be neglected as well. Then the second nonlinear crystal acts on the second pump photon and at point 2 we fill find

$$\begin{aligned}|\text{in}\rangle &= \frac{1}{\sqrt{2}}(\alpha\, t\mathrm{e}^{\mathrm{i}\theta}\hat{a}^\dagger_{s_1}\hat{a}^\dagger_{i_1} + \mathrm{i}\hat{a}^\dagger_{p_2})\,|0\rangle \\ &\xrightarrow{2} \frac{1}{\sqrt{2}}(\alpha\, t\mathrm{e}^{\mathrm{i}\theta}\hat{a}^\dagger_{s_1}\hat{a}^\dagger_{i_1} + \alpha\mathrm{i}\hat{a}^\dagger_{s_2}\hat{a}^\dagger_{i_2})\,|0\rangle\,.\end{aligned} \tag{4.15}$$

Since both idler paths are spatially perfectly overlapping we can set $\hat{a}^\dagger_{i_1} = \hat{a}^\dagger_{i_2} = \hat{a}^\dagger_i$. At point 3 both signal paths will again be mixed via a beam splitter which also adds an additional phase

$\Delta\varphi$

$$\begin{aligned}
&\xrightarrow{2} \frac{\alpha}{\sqrt{2}}(t\mathrm{e}^{\mathrm{i}\theta}\hat{a}^\dagger_{s_1} + \mathrm{i}\hat{a}^\dagger_{s_2})\hat{a}^\dagger_i|0\rangle \\
&\xrightarrow{3} \frac{\alpha}{\sqrt{2}}(t\mathrm{e}^{\mathrm{i}\theta}\hat{a}^\dagger_{s_1} + \mathrm{i}\mathrm{e}^{\mathrm{i}\Delta\varphi}\hat{a}^\dagger_{s_2})\hat{a}^\dagger_i|0\rangle \\
&\xrightarrow{4} \frac{\alpha}{\sqrt{2}}\left(t\mathrm{e}^{\mathrm{i}\theta}\frac{1}{\sqrt{2}}(\mathrm{i}\hat{a}^\dagger_{d_1} + \hat{a}^\dagger_{d_2}) + \mathrm{i}\mathrm{e}^{\mathrm{i}\Delta\varphi}\frac{1}{\sqrt{2}}(\hat{a}^\dagger_{d_1} + \mathrm{i}\hat{a}^\dagger_{d_2})\right)\hat{a}^\dagger_i|0\rangle \\
&= \frac{\alpha}{2}\left(t\mathrm{e}^{\mathrm{i}\theta}(\mathrm{i}\hat{a}^\dagger_{d_1} + \hat{a}^\dagger_{d_2}) + \mathrm{e}^{\mathrm{i}\Delta\varphi}(\mathrm{i}\hat{a}^\dagger_{d_1} - \hat{a}^\dagger_{d_2})\right)\hat{a}^\dagger_i|0\rangle \\
|\mathrm{out}\rangle &= \frac{\alpha}{2}\left[\left(t\mathrm{e}^{\mathrm{i}\theta} + \mathrm{e}^{\mathrm{i}\Delta\varphi}\right)\mathrm{i}\hat{a}^\dagger_{d_1} + \left(t\mathrm{e}^{\mathrm{i}\theta} - \mathrm{e}^{\mathrm{i}\Delta\varphi}\right)\hat{a}^\dagger_{d_2}\right]\hat{a}^\dagger_i|0\rangle\,. \qquad (4.16)
\end{aligned}$$

Now, the probability to detect a signal photon in detectors D_1 and D_2 is ($t \in \mathbb{R}$)

$$\begin{aligned}
P_{D_1} &= \frac{|\alpha|^2}{4}|t\mathrm{e}^{\mathrm{i}\theta} + \mathrm{e}^{\mathrm{i}\Delta\varphi}|^2 = \frac{|\alpha|^2}{4}\left(|t|^2 + 1 + t\mathrm{e}^{\mathrm{i}(\theta-\Delta\varphi)} + t\mathrm{e}^{-i(\theta-\Delta\varphi)}\right) \\
&= \frac{|\alpha|^2}{4}\left(1 + |t|^2 + 2t\cos\left(\theta - \Delta\varphi\right)\right) \qquad (4.17) \\
P_{D_2} &= \frac{|\alpha|^2}{4}\left(1 + |t|^2 - 2t\cos\left(\theta - \Delta\varphi\right)\right). \qquad (4.18)
\end{aligned}$$

This result corresponds well with the measurements performed in figure 16. For $t = 0$ we will have a constant probability independent on $\Delta\varphi$, whereas for $t \neq 0$ we observe a sinusoidal behavior as expected.

4.3 Dispersion cancellation

In the following we want to discuss the effect of dispersion cancellation in a two-photon interference setup. For a dispersive medium the dispersion relation is given as

$$k(\omega) = \frac{n(\omega)\omega}{c}. \qquad (4.19)$$

We now want to perform a Taylor series expansion around a mean frequency ω_0 giving us

$$k(\omega) = k_0 + \alpha(\omega - \omega_0) + \beta(\omega - \omega_0)^2 + \ldots \qquad (4.20)$$

When a wave packet is traveling through a dispersive medium of length L, it will acquire a phase shift

$$\varphi(\omega) = k(\omega)\cdot L = \varphi_0 + \alpha L(\omega - \omega_0) + \underbrace{\beta L}_{\propto \mathrm{GDD}}(\omega - \omega_0)^2. \qquad (4.21)$$

The prefactor of the second term is proportional to the group delay dispersion (GDD) which is responsible for dispersive pulse broadening effects according to

$$\tau = \tau_0\sqrt{1 + \left(4\ln 2\frac{\mathrm{GDD}}{\tau_0^2}\right)^2}, \quad \text{where } \tau_0 \text{ is FWHM for a Gaussian.} \qquad (4.22)$$

Now we consider a HOM interferometer as sketched in figure 9 with a dispersive element in the signal arm. The frequency entangled state from the SPDC process is given as

$$\left|\psi\right\rangle = \int \mathrm{d}\omega\, \Phi(\omega)\, |\omega_0+\omega, \omega_0-\omega\rangle\,, \tag{4.23}$$

where $\Phi(\omega)$ is the two-photon spectral amplitude function and ω describes the deviation about the central angular frequency ω_0 of the twin-photon wave packet. The ladder operators for the detector modes D_1 and D_2 are given as

$$\begin{aligned}\hat{a}_1(\omega) &= \frac{1}{\sqrt{2}}\left(\mathrm{i}\hat{a}_s(\omega)\mathrm{e}^{\mathrm{i}k(\omega)L} + \hat{a}_i(\omega)\mathrm{e}^{\mathrm{i}\omega\frac{\delta l}{c}}\right)\\ \hat{a}_2(\omega) &= \frac{1}{\sqrt{2}}\left(\hat{a}_s(\omega)\mathrm{e}^{\mathrm{i}k(\omega)L} + \mathrm{i}\hat{a}_i(\omega)\mathrm{e}^{\mathrm{i}\omega\frac{\delta l}{c}}\right),\end{aligned} \tag{4.24}$$

where δl is the displacement of the mirror (now in idler path). Note that the following commutator relations hold:

$$[\hat{a}_j(\omega), \hat{a}_k^\dagger(\omega')] = \delta_{jk}\delta(\omega-\omega'), \qquad [\hat{a}_j(\omega), \hat{a}_k(\omega)] = 0. \tag{4.25}$$

Hence, the positive and negative frequency parts of the electric field at detector $j = 1,2$ are given by

$$\hat{E}_j^{(+)}(t) = \int \mathrm{d}\omega\, \hat{a}_j(\omega^*)\mathrm{e}^{-\mathrm{i}\omega^* t} \quad \text{and} \quad \hat{E}_j^{(-)}(t) = \int \mathrm{d}\omega\, \hat{a}_j^\dagger(\omega)\mathrm{e}^{\mathrm{i}\omega t} = \left[\hat{E}_j^{(+)}(t)\right]^\dagger. \tag{4.26}$$

Now we can compare the coincidence rates (which are proportional to $g^{(2)}$)

$$R_c = \int_0^T \mathrm{d}t_1\, \mathrm{d}t_2 \left\langle \psi|\hat{E}_1^{(-)}(t_1)\hat{E}_2^{(-)}(t_2)\hat{E}_1^{(+)}(t_1)\hat{E}_2^{(+)}(t_2)|\psi\right\rangle. \tag{4.27}$$

Here we have to perform four frequency integrations. However, since the time window for coincidences is much longer than the coherence length $1/\Delta\omega$, the interaction time is effectively infinity

$$\lim_{T\to\infty}\int_0^T \mathrm{d}t\, \mathrm{e}^{\mathrm{i}t(\omega^- - \omega^+)} \approx \delta(\omega^- - \omega^+). \tag{4.28}$$

Then the coincidence rate can be calculated to

$$\begin{aligned} R_c &= \iint \mathrm{d}\omega_1\, \mathrm{d}\omega_2 \underbrace{\left\langle \psi|\hat{a}_1^\dagger(\omega_1)\hat{a}_2^\dagger(\omega_2)\hat{a}_1(\omega_1)\hat{a}_2(\omega_2)|\psi\right\rangle}\\ &= \sum_n \left\langle \psi|\hat{a}_1^\dagger\hat{a}_2^\dagger|n\right\rangle\left\langle n|\hat{a}_1\hat{a}_2|\psi\right\rangle\\ &\overset{*}{=} \sum_n \left\langle \psi|\hat{a}_1^\dagger\hat{a}_2^\dagger|0\right\rangle\left\langle 0|\hat{a}_1\hat{a}_2|\psi\right\rangle = |\left\langle 0|\hat{a}_1\hat{a}_2|\psi\right\rangle|^2\\ &\overset{(4.24)}{=} \left|\frac{1}{2}\left\langle 0|\hat{a}_i(\omega_1)\hat{a}_s(\omega_2)\mathrm{e}^{\mathrm{i}\omega_1\frac{\delta l}{c}+\mathrm{i}k(\omega_2)L} - \hat{a}_s(\omega_1)\hat{a}_i(\omega_2)\mathrm{e}^{\mathrm{i}\omega_2\frac{\delta l}{c}+\mathrm{i}k(\omega_1)L}|\psi\right\rangle\right|^2 \end{aligned} \tag{4.29}$$

$$\overset{(4.20)}{=} \left|\frac{1}{2}\delta(\omega_p-\omega_1-\omega_2)\Phi(\omega')\mathrm{e}^{\mathrm{i}\omega_p\frac{\delta l}{c}+\mathrm{i}k(\omega_p)L}\left(\mathrm{e}^{-\mathrm{i}\omega'\frac{\delta l}{c}+\mathrm{i}L(-\alpha\omega'+\beta\omega'^2)}-\mathrm{e}^{\mathrm{i}\omega'\frac{\delta l}{c}+\mathrm{i}L(\alpha\omega'+\beta\omega'^2)}\right)\right|$$

$$= \frac{1}{4}|\delta(\omega_p-\omega_1-\omega_2)|^2|\Phi(\omega')|^2\left[2-2\,\mathrm{Re}\left(\mathrm{e}^{2\mathrm{i}\omega'\frac{\delta l}{c}-2\mathrm{i}\alpha\omega' L}\right)\right] \quad \text{with} \quad \omega'=\omega_1-\omega_p$$

$$R_c = \int \mathrm{d}\omega'\,|\Phi(\omega')|^2\left[1-\cos\left(2\omega'\left(\frac{\delta l}{c}-\alpha L\right)\right)\right]. \tag{4.30}$$

In the third line we used that for a photon pair state only $n=0$ contributes in the sum. We observe that the contribution of β vanishes in the second to last line. Therefore the coincidence rate is dispersion insensitive and we only have group delay dependence.

4.4 Classical optical coherence tomography

We now consider a light source with low temporal coherence length, i. e. a broad spectrum. This may be an ultrashort pulse or a white light source. We take a Michelson interferometer setup as depicted in figure 17. Then one mirror is exchanged by a sample. We model the beam passage through the sample by a transfer function

$$H(\omega) = \int_0^\infty \mathrm{d}z\, r(z,\omega)\mathrm{e}^{2\mathrm{i}\varphi(z,\omega)}, \tag{4.31}$$

where r is the reflection coefficient of the sample. The factor of two in the phase is considering forward and back propagation in the sample. For a broadband light source with $\omega=\omega_0+\Omega$ and spectral power density $S(\omega)\sim I_0$, the intensity at the detector is given by

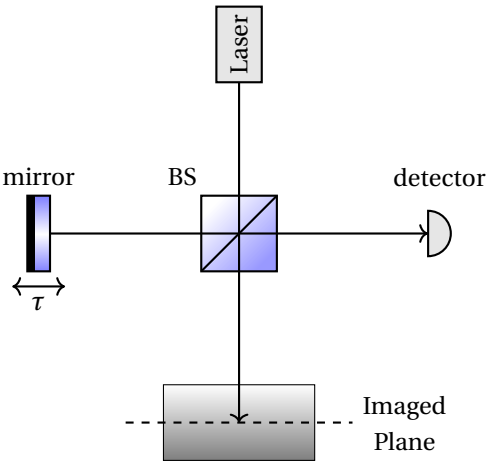

Fig. 17: Optical coherence tomography. Michelson interferometer setup.

$$I = \left\langle|E_r+E_s|^2\right\rangle = \frac{1}{2}(I_r+I_s)+\mathrm{Re}[\left\langle(E_r^*(t+\tau))E_s(t)\right\rangle]. \tag{4.32}$$

Here E_r and E_s are the fields of the reference and sample respectively. We can also write this as

$$I(\tau)\sim \overbrace{\Gamma_0}^{\text{self interference}} + 2\underbrace{\mathrm{Re}[\Gamma(\tau)\mathrm{e}^{-\mathrm{i}\omega\tau}]}_{\text{cross intereference}}, \tag{4.33}$$

where the new quantities Γ_0 and $\Gamma(\tau)$ are given by

$$\Gamma_0 = \int \mathrm{d}\Omega\,(1+|H(\omega_0+\Omega)|^2)S(\Omega), \quad \text{and} \quad \Gamma(\tau) = \int \mathrm{d}\Omega\, H(\omega_0+\Omega)S(\Omega)\mathrm{e}^{-\mathrm{i}\Omega t} = \gamma^{(1)}(\tau). \tag{4.34}$$

In the last equal sign we used the WIENER-KHINCHINE theorem again (3.24).

The procedure for performing a classical OCT experiment is as follows:

- Determine the spectral density $S(\omega)$ which is given by the light source.
- Measure Γ_0 and $\Gamma(\tau)$.
- Then we can obtain the transfer function $H(\omega)$ and can extract the reflection coefficient $r(z,\omega)$.

However, OCT experiments are limited by the group velocity dispersion (GVD) of the sample.

Quantum OCT

We can solve the problem of dispersion and increase our resolution by performing a quantum optical coherence tomography experiment. We take a setup similar to figure 9 as shown in figure 18.

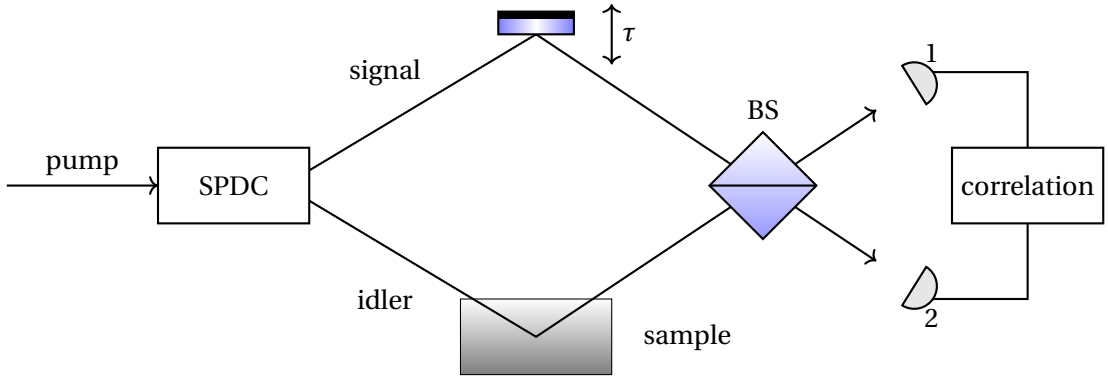

Fig. 18: Signal and idler photons produced by a type-I phase matching SPDC process are used to perform a quantum OCT experiment.

The light source is now a SPDC source with $\omega_\pm = \omega_0 \pm \Omega$. Analogous to equation (4.23) the state can be written as

$$\left|\psi\right\rangle = \int \mathrm{d}\Omega\, \Phi(\Omega)\, \left|\omega_0+\Omega, \omega_0-\Omega\right\rangle, \quad \text{with} \quad |\Phi(\Omega)|^2 = S(\Omega) \quad \text{and} \quad \int \mathrm{d}\Omega\, S(\Omega) = 1. \tag{4.35}$$

The coincidence rate is now given by

$$C(\tau) \sim \Lambda_0 - \mathrm{Re}[\Lambda(2\tau)], \quad \text{with} \tag{4.36}$$
$$\Lambda_0 = \int \mathrm{d}\Omega\, |H(\omega_0+\Omega)|^2 S(\Omega), \quad \text{and} \quad \Lambda(\tau) = \int \mathrm{d}\Omega\, H(\omega_0+\Omega) H^*(\omega_0-\Omega) S(\Omega) \mathrm{e}^{\mathrm{i}\Omega t}.$$

Note that there are similarities to the expressions found in the classical case (equations (4.33) and (4.34)). However, there are some differences. Since we probe the sample with both frequencies we can actually achieve a doubling of the resolution. Furthermore we can make use of dispersion cancellation.

4.5 Franson interferometer

We recall that for the HOM effect both photons do not need to arrive at the same time at the BS. The indistinguishability, however, of the RR (reflected, reflected) and TT (transmitted, transmitted) case are essential. We observe a similar behavior in the Franson interferometer sketched in figure 19.

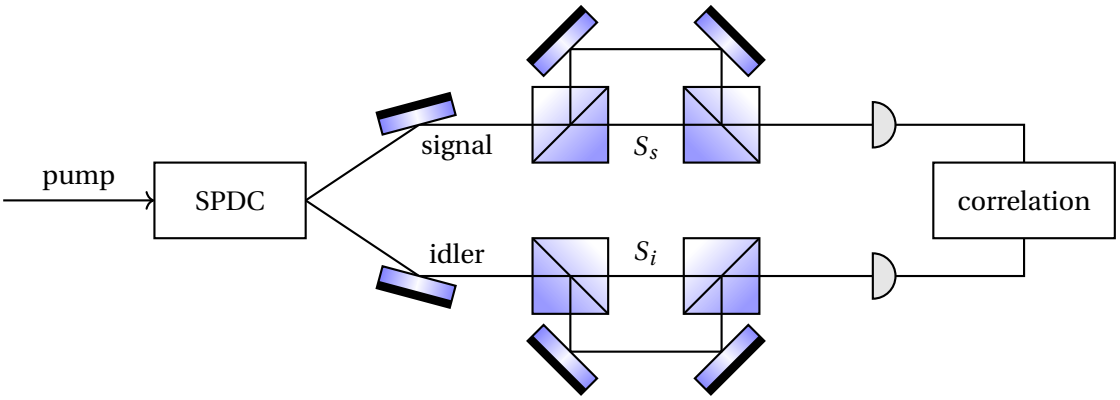

Fig. 19: Franson interferometer setup.

The path length difference between short (S) and long (L) path is much larger than the coherence length of signal and idler photons. We have four options the signal and idler photons can take:

$$L_sL_i, \quad \underbrace{L_sS_i, \quad S_sL_i}_{\text{can be neglected}} \quad \text{and} \quad S_sS_i. \tag{4.37}$$

Two cases can be neglected for coincidences if the acquisition time of the detectors is smaller than time difference of long and short path. However, L_sL_i and S_sS_i are indistinguishable options and will interfere

$$\left|\psi\right\rangle = \frac{1}{2}\left(\left|S\right\rangle_s\left|S\right\rangle_i + \mathrm{e}^{\mathrm{i}\varphi}\left|L\right\rangle_s\left|L\right\rangle_i\right). \tag{4.38}$$

Let Δl_s and Δl_i be the path difference between the long and short path for signal and idler. Then the phase difference between LL and SS path is

$$\begin{aligned}\varphi &= \frac{\omega_s\Delta l_s}{c} + \frac{\omega_i\Delta l_i}{c} = \frac{\overbrace{\omega_s+\omega_i}^{=\omega_p}}{2}(\Delta l_s + \Delta l_i) + \frac{\overbrace{\omega_s-\omega_i}^{\approx 0}}{2}(\Delta l_s - \Delta l_i)\\ \varphi &\approx \frac{1}{2}\omega_p(\Delta l_i + \Delta l_s).\end{aligned} \tag{4.39}$$

The probability of coincidences is now

$$\begin{aligned}P_C &= \left|\left\langle\psi\middle|\psi\right\rangle\right|^2 = \frac{1}{4}\left|1+\mathrm{e}^{\mathrm{i}\varphi}\right|^2 = \frac{1}{2}(1+\cos\varphi)\\ &= \frac{1}{2}\left[1+\cos\left(\frac{\omega_p}{2}(\Delta l_s + \Delta l_i)\right)\right].\end{aligned} \tag{4.40}$$

We conclude that 100 % visibility is possible although the photons never interacted with each other. This leads us to the concept of time bin entanglement.

5 Quantum metrology

5.1 Absolute calibration of photon detectors

In the following we consider a simple detector setup with a nonlinear crystal creating a signal and idler beam. Both are detected by detectors D_1 and D_2 respectively. The number of photon pairs sent out is called N and $N_i = \eta_i N$ is the actual number of photons detected. Here we defined a detection efficiency η_i for every detector. This scenario is depicted in figure 20. Now we want to find the detection efficiency η_1 while detector D_2 has an *unknown* efficiency η_2. The total coincidence rate N_C is

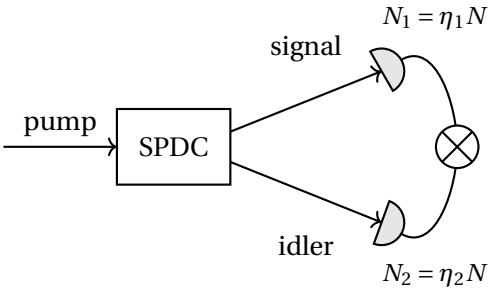

Fig. 20: Simple detector setup.

$$N_c = \eta_1 \eta_2 N = \eta_1 N_2 \quad \Rightarrow \quad \eta_1 = \frac{N_c}{N_2}. \tag{5.1}$$

This calculation is independent of η_2.

5.2 Phase measurements and limits

5.2.1 Interferometry with coherent states

We now consider a Mach Zehnder interferometer with a coherent state on port 2 and vacuum on port 1 as depicted in figure 21. Since the coherent state can describe classical laser light (perfect coherence) we expect to retain the behavior known from classical interferometry. The coherent state input is transformed as

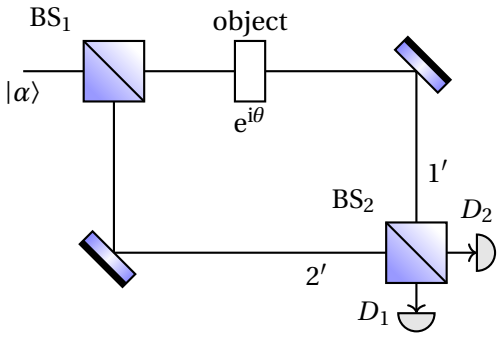

Fig. 21: Mach Zehnder interferometer with coherent state in port 2.

$$|0\rangle|\alpha\rangle \xrightarrow{\text{BS}} \left|\frac{i\alpha}{\sqrt{2}}\right\rangle \left|\frac{\alpha}{\sqrt{2}}\right\rangle \quad (\bar{n} = \langle\hat{n}\rangle = |\alpha|^2) \tag{5.2}$$

The phase shifting object yields

$$\left|\frac{i\alpha}{\sqrt{2}}\right\rangle_{1''} \left|\frac{\alpha}{\sqrt{2}}\right\rangle_{2''} \xrightarrow{\theta} \left|\frac{ie^{i\theta}\alpha}{\sqrt{2}}\right\rangle_{1'} \left|\frac{\alpha}{\sqrt{2}}\right\rangle_{2'} \tag{5.3}$$

The second BS transforms as follows

$$\left|\frac{ie^{i\theta}\alpha}{\sqrt{2}}\right\rangle_{1'} \left|\frac{\alpha}{\sqrt{2}}\right\rangle_{2'} \xrightarrow{\text{BS}} \left|\frac{i(e^{i\theta}+1)\alpha}{\sqrt{2}}\right\rangle_{1} \left|\frac{(e^{i\theta}-1)\alpha}{\sqrt{2}}\right\rangle_{2} = |\psi\rangle. \tag{5.4}$$

The output probability at detector $D_{1,2}$ is then ($\bar{n} = |\alpha|^2$)

$$\begin{aligned}\langle \hat{n}_1 \rangle &= \langle \psi | \hat{n}_1 | \psi \rangle = \left| \frac{\mathrm{i}}{\sqrt{2}} (\mathrm{e}^{\mathrm{i}\theta} + 1)\alpha \right|^2 = \frac{\bar{n}}{2}(1+\cos\theta) \\ \langle \hat{n}_2 \rangle &= \langle \psi | \hat{n}_2 | \psi \rangle = \left| \frac{\mathrm{i}}{\sqrt{2}} (\mathrm{e}^{\mathrm{i}\theta} - 1)\alpha \right|^2 = \frac{\bar{n}}{2}(1-\cos\theta).\end{aligned} \tag{5.5}$$

We can obtain the best contrast by subtracting both outputs via an operator $\hat{O}$

$$\hat{O} := \hat{n}_1 - \hat{n}_2 \quad \Rightarrow \langle \hat{O} \rangle = \bar{n}_1 - \bar{n}_2 = \bar{n}\cos\theta. \tag{5.6}$$

Now we may ask how precise can θ be measured or rather how large is its uncertainty $\Delta\theta$. Let us consider the uncertainty of $\hat{O}$ first

$$\begin{aligned}\Delta\hat{O} &= \sqrt{\underbrace{\langle \hat{O}^2 \rangle} - \langle \hat{O} \rangle^2} \\ &\langle \hat{O}^2 \rangle = \langle \psi | (\hat{n}_1 - \hat{n}_2)^2 | \psi \rangle = \underbrace{\langle \hat{n}_1^2 \rangle}_{\bar{n}_1^2 + \bar{n}_1} + \underbrace{\langle \hat{n}_2^2 \rangle}_{\bar{n}_2^2 + \bar{n}_2} - 2\underbrace{\langle \hat{n}_1 \hat{n}_2 \rangle}_{\bar{n}_1 \bar{n}_2} \\ &\langle \hat{O}^2 \rangle = (\bar{n}_1 - \bar{n}_2)^2 + \bar{n}_1 + \bar{n}_2 = \bar{n}^2 \cos^2\theta + \bar{n} \\ \Delta\hat{O} &= \sqrt{\bar{n}^2\cos^2\theta + \bar{n} - \bar{n}^2\cos^2\theta} = \sqrt{\bar{n}}.\end{aligned} \tag{5.7}$$

We can now perform an uncertainty calculation of $\hat{O}$

$$\Delta\hat{O} = \left| \frac{\partial \langle \hat{O} \rangle}{\partial\theta} \right| \Delta\theta = \left| \frac{\mathrm{d}(\bar{n}\cos\theta)}{\mathrm{d}\theta} \right| \Delta\theta = \bar{n}|\sin\theta|\Delta\theta. \tag{5.8}$$

Thus we find for the uncertainty of θ

$$\Delta\theta = \frac{\Delta\hat{O}}{\bar{n}|\sin\theta|} \overset{(5.7)}{=} \frac{1}{\sqrt{\bar{n}}|\sin\theta|}. \tag{5.9}$$

The uncertainty is minimal at $\theta = \frac{\pi}{2}$

$$\Delta\theta_{\min} = \frac{1}{\sqrt{\bar{n}}}. \tag{5.10}$$

This result corresponds to the standard quantum limit, the *shot noise limit*. The more photons we detect, the better our measurement. Here noise is less important. Utilizing this technique is relevant for the detection of e. g. gravitational waves.

5.2.2 Interferometry with NOON states

A NOON state is a quantum-mechanical many-body entangled photon state representing a superposition of N particles in one mode and zero particles in the other mode. The state is given as

$$\begin{aligned}|\psi\rangle_{\text{NOON}} &= \frac{1}{\sqrt{2}}\left(|N,0\rangle + \mathrm{e}^{\mathrm{i}\theta}|0,N\rangle\right) \\ &= \frac{1}{\sqrt{2}}((\hat{a}_1^\dagger)^N + \mathrm{e}^{\mathrm{i}\theta}(\hat{a}_2^\dagger)^N)|0\rangle\,. \quad (5.11)\end{aligned}$$

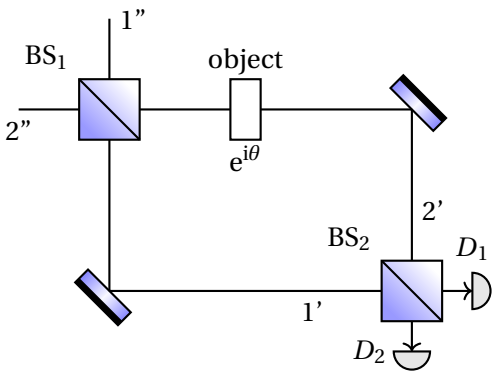

Fig. 22: Mach Zehnder interferometer setup.

The special case $N = 2$ corresponds to the HOM-experiment of an entangled two-photon state. Again we consider the Mach Zehnder interferometer as depicted in figure 22. The transformation of the ladder operators after the first beam splitter is given by

$$\begin{aligned}&\hat{a}_{1''}^\dagger \to \frac{1}{\sqrt{2}}(\hat{a}_{1'}^\dagger + \mathrm{i}\hat{a}_{2'}^\dagger) \quad \text{and} \quad \hat{a}_{2''}^\dagger \to \frac{1}{\sqrt{2}}(\mathrm{i}\hat{a}_{1'}^\dagger + \hat{a}_{2'}^\dagger) \\ &\text{state:} \quad \frac{\mathrm{i}}{2}\left[(\hat{a}_{1'}^\dagger)^2 + (\hat{a}_{2'}^\dagger)^2\right]|0\rangle\,. \quad (5.12)\end{aligned}$$

This corresponds two the HOM effect of the entangled two-photon state behind a single beam splitter (c. f. equation (3.46)). Now we can further calculate the state after the phase object $\hat{a}_{2'}^\dagger \to \mathrm{e}^{\mathrm{i}\theta}\hat{a}_{2'}^\dagger$

$$|\psi\rangle_{\text{object}} = \frac{\mathrm{i}}{2}\left[(\hat{a}_{1'}^\dagger)^2 + \mathrm{e}^{2\mathrm{i}\theta}(\hat{a}_{2'}^\dagger)^2\right]|0\rangle\,. \quad (5.13)$$

The factor of two in the phase term is a different result to the classical case. Then the second beam splitter acts on this state resulting in a final state of

$$|\psi\rangle_{\text{out}} = \Big[\underbrace{\frac{\mathrm{i}}{4}(1-\mathrm{e}^{2\mathrm{i}\theta})[(\hat{a}_1^\dagger)^2 - (\hat{a}_2^\dagger)^2]}_{\text{no coincidences}} - \underbrace{\frac{1}{2}(1+\mathrm{e}^{2\mathrm{i}\theta})\hat{a}_1^\dagger\hat{a}_2^\dagger}_{\text{coincidences}}\Big]|0\rangle\,. \quad (5.14)$$

Now let us define an operator that picks out the coincidences

$$\hat{C}_1 := \hat{a}_1^\dagger\hat{a}_2^\dagger\hat{a}_2\hat{a}_1, \qquad \langle\hat{C}_1\rangle = \left|\frac{1}{2}\left(1+\mathrm{e}^{2\mathrm{i}\theta}\right)\right|^2 = \frac{1}{2}[1+\cos(2\theta)]. \quad (5.15)$$

Furthermore we also define an operator that picks out events without coincidences

$$\hat{C}_2 = \frac{1}{2}\hat{n} - \hat{C}_1 = \frac{1}{2}(\hat{n}_1 + \hat{n}_2) - \hat{C}_1. \quad (5.16)$$

The factor $\frac{1}{2}$ balances with the expectation value $\langle\hat{n}\rangle = 2$. Note that $\langle\hat{C}_2 + \hat{C}_1\rangle = 1$. Now we take the difference of both operators

$$\hat{C} := \hat{C}_1 - \hat{C}_2, \quad \langle\hat{C}\rangle = \langle 2\hat{C}_1\rangle - \frac{1}{2}\langle\hat{n}\rangle = \cos(2\theta). \quad (5.17)$$

Leading up to the uncertainty of $\hat{C}$ we first determine the expectation value of $\hat{C}^2$

$$\begin{aligned}\langle\hat{C}^2\rangle &= \langle\psi|(\hat{C}_1-\hat{C}_2)^2|\psi\rangle \\ &= \underbrace{\langle\hat{C}_1^2\rangle} + \langle\hat{C}_2^2\rangle - \underbrace{\langle\hat{C}_1\hat{C}_2\rangle}_{=0} - \underbrace{\langle\hat{C}_2\hat{C}_1\rangle}_{=0} \qquad (5.18)\\ &= \left|\frac{1}{2}(1+\mathrm{e}^{2\mathrm{i}\theta})\right|^2 \left\langle \underbrace{0|\hat{a}_2\hat{a}_1}_{\langle\psi|}\underbrace{\hat{a}_1^\dagger\hat{a}_2^\dagger\hat{a}_2\hat{a}_1}_{\hat{C}_1}\underbrace{\hat{a}_1^\dagger\hat{a}_2^\dagger\hat{a}_2\hat{a}_1}_{\hat{C}_1}\underbrace{\hat{a}_1^\dagger\hat{a}_2^\dagger|0}_{|\psi\rangle}\right\rangle \\ &= \left|\frac{1}{2}(1+\mathrm{e}^{2\mathrm{i}\theta})\right|^2 \underbrace{\langle 0|0\rangle}_{=1} = \langle\hat{C}_1\rangle \\ &= \langle\hat{C}_1\rangle + \langle\hat{C}_2\rangle = 1 \quad \text{no squares anymore.} \qquad (5.19)\end{aligned}$$

Hence, the uncertainty of $\hat{C}$ is

$$\Delta\hat{C} = \sqrt{\langle\hat{C}^2\rangle - \langle\hat{C}\rangle^2} = \sqrt{1-\cos^2(2\theta)} = |\sin(2\theta)|. \qquad (5.20)$$

$$\text{Also} \quad \Delta\hat{C} = \left|\frac{\partial\langle\hat{C}\rangle}{\partial\theta}\right|\Delta\theta = \left|\frac{\partial\cos(2\theta)}{\partial\theta}\right|\Delta\theta = 2|\sin(2\theta)|\Delta\theta. \qquad (5.21)$$

Therefore we find for the phase uncertainty

$$\Delta\theta = \frac{1}{2} \quad \text{for two photons.} \qquad (5.22)$$

If we now generalize this calculation to NOON states $N>2$ we find

$$\Delta\theta_H = \frac{1}{N} = \frac{1}{\sqrt{N}}\frac{1}{\sqrt{N}} \overset{(5.10)}{=} \Delta_{\mathrm{SQL}}\frac{1}{\sqrt{N}}, \quad \text{with} \quad \bar{n}=N. \qquad (5.23)$$

This limit is called *Heisenberg limit* and reduces the standard quantum limit by a factor of $1/\sqrt{N}$. We observe that the uncertainty of quantum states is lower than for classical states (e. g. coherent states). Note, that in a generalized NOON state

$$|\psi\rangle \sim |N,0\rangle + \mathrm{e}^{\mathrm{i}N\theta}|0,N\rangle, \qquad (5.24)$$

the phase oscillates with $N\theta$ which leads to a higher precision/sensitivity since the interference fringes oscillate N times faster.

However, there is a catch. The production of NOON states is very difficult.

6 Correlation-based quantum imaging

6.1 Sub-shot noise imaging

Our aim in this chapter will be the imaging of a 2D object. This is basically a measurement of transmission/reflection of the object with spatial resolution. First we want to analyze simple transmission measurements. Here we consider (as shown in figure 23) $\langle \hat{n} \rangle$ as the expectation value of the incoming photon number and $\langle \hat{N} \rangle$ as the expectation value of the measured photon number. Assuming an absorbing object with absorption α, the transmission is given by

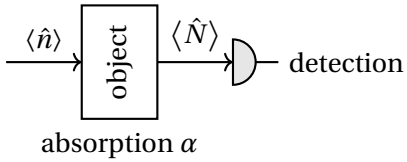

Fig. 23: Schematic drawing of the problem.

$$T = 1 - \alpha, \quad \Rightarrow \quad \langle \hat{N} \rangle = (1 - \alpha) \langle \hat{n} \rangle . \tag{6.1}$$

The absorption can now be measured with a single detector if $\langle \hat{n} \rangle$ is known. The uncertainty of absorption is given by

$$\Delta\alpha = \frac{\Delta\hat{N}}{\frac{\partial \langle \hat{N} \rangle}{\partial \alpha}} \quad \text{with} \quad \Delta\hat{N} = \sqrt{\langle \hat{N}^2 \rangle - \langle \hat{N} \rangle^2}. \tag{6.2}$$

The uncertainty $\Delta\alpha$ depends on the sensitivity on $\langle \hat{N} \rangle$. The variance of $\hat{N}$ is given as

$$(\Delta\hat{N})^2 = (1-\alpha)^2 \underbrace{[(\Delta\hat{n})^2 - \langle \hat{n} \rangle]}_{\text{linked to statistics of the input beam}} + (1-\alpha) \langle \hat{n} \rangle . \tag{6.3}$$

We want sketch a way on how to derive equation (6.3). The connection between the output operators $\hat{b}$ and the input operators $\hat{a}$ for the photon source and $\hat{v}$ for the vacuum is given by

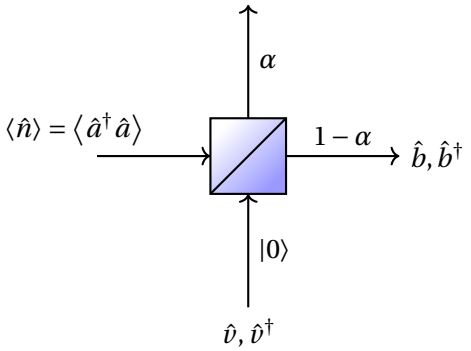

Fig. 24: Sketch for deriving equation (6.3).

$$\hat{b} = \sqrt{1-\alpha}\,\hat{a} + \mathrm{i}\sqrt{\alpha}\,\hat{v}. \tag{6.4}$$

The variance $(\Delta\hat{N})^2$ is given by

$$(\Delta\hat{N})^2 = \langle \hat{N}^2 \rangle - \langle \hat{N} \rangle^2 = \left\langle \hat{b}^\dagger \hat{b} \hat{b}^\dagger \hat{b} \right\rangle - \left\langle \hat{b}^\dagger \hat{b} \right\rangle^2 . \tag{6.5}$$

If we now put in equation (6.4) and use the respective commutation relations, a connection between $(\Delta\hat{N})^2$ and $(\Delta\hat{n})^2$ will appear.

We can characterize the statistics of a given state using the *Mandel parameter*

$$Q = \frac{(\Delta\hat{n})^2 - \langle \hat{n} \rangle}{\langle \hat{n} \rangle} = \frac{(\Delta\hat{n})^2}{\langle \hat{n} \rangle} - 1 = F - 1, \tag{6.6}$$

where F is the *Fano parameter*. The we can distinguish between different cases:

$$\begin{cases} F > 1 & \text{Classical states, super-Poissonian statistics} \\ F = 1 & \text{Coherent state, Poissonian statistics} \\ F < 1 & \text{Non-classical states, sub-Poissonian statistics} \end{cases} \tag{6.7}$$

We can now put everything together into an equation for the measured uncertainty:

$$\Delta\alpha = \sqrt{\frac{(1-\alpha)^2(F-1)+(1-\alpha)}{\langle\hat{n}\rangle}}, \tag{6.8}$$

which is also displayed in figure 25 for different Fano parameters. We observe that the advantage of using quantum states is largest for small values of absorption α. In case of a number state ($F = 0$) we find the biggest possible advantage compared to classical states. In contrast to the NOON states, this is practically applicable, as the number states can be generated for $\langle\hat{n}\rangle = 1, 2$.

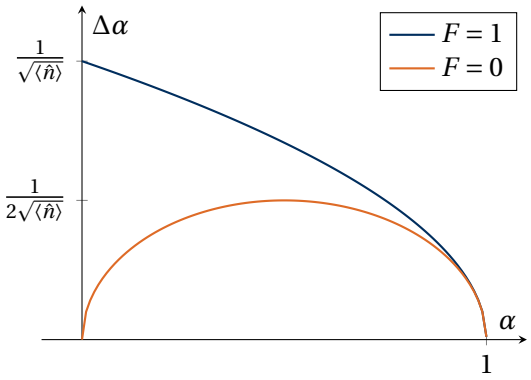

Fig. 25: Uncertainty $\Delta\alpha$ for different Fano parameters.

However, there is a problem, namely the limited efficiency η of our detectors. This acts like an additional loss term and reduces the nonclassicality and the Fano parameter to a lower bound of $F_{\text{det}} = 1 - \eta$.

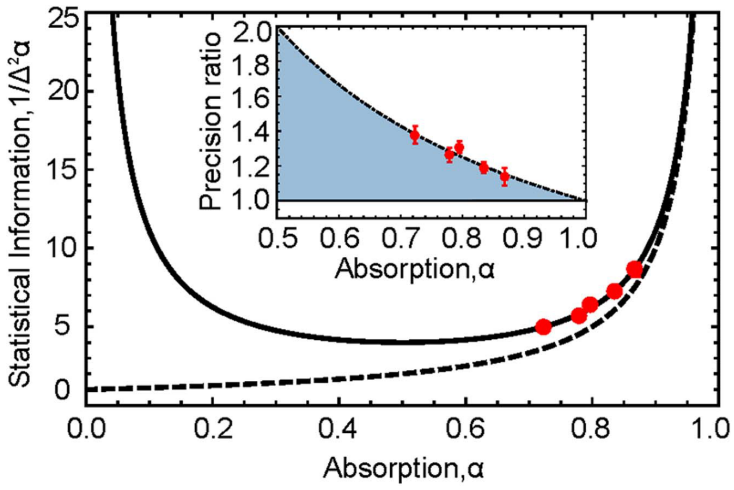

Fig. 26: Estimating the overall loss α. The Fock state $|1\rangle$ is represented by the solid line and the coherent state with same average intensity by the dashed line (SNL). The divergence at $\alpha = 0, 1$ corresponds to vanishing variance.
Inset: The dotted-dashed line corresponds to the ideal quantum advantage obtained by $|1\rangle$, defined by the precision ratio of $\Delta^2\alpha$ for the Fock and coherent state. The data points (red) are take at fixed wavelengths using ND-filters to simulate loss.
Taken from: R Whittaker et al 2017 New J. Phys. 19 023013

Indeed this approach has been used for measurements as shown in figure 26. The close agreement with the theoretical limit evidences the potential for using single photons to reach

the ultimate levels in precision for absorption spectroscopy (c. f. figure 27). Since α is the overall absorption, the gain in precision over the SNL is limited by components such as detectors, motivating the need for increased efficiency photon-pair sources and single photon detectors.

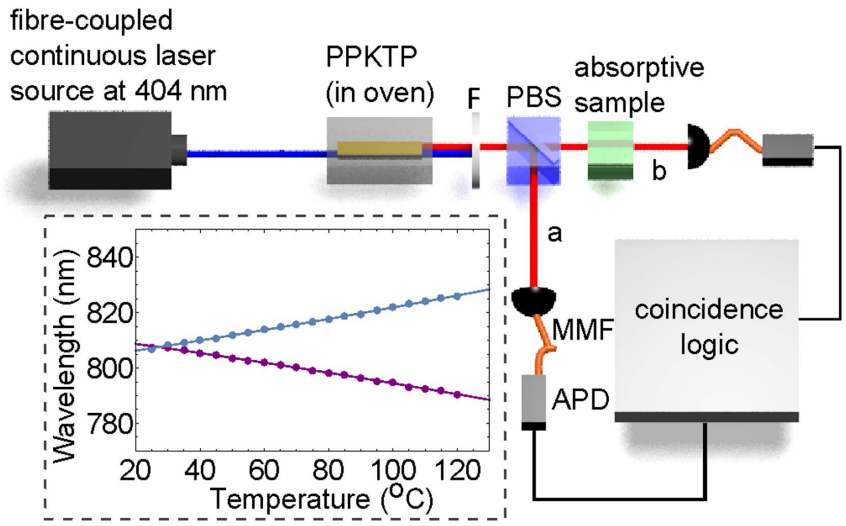

Fig. 27: Setup for sub-shot-noise spectroscopy. Wavelength correlated photon pairs are generated using a laser to pump a NL crystal (PPKTP) phase-matched for collinear type-II SPDC and temperature tuned for wavelength control. MMf-multimode fibre; APD-avalanche photo diode; F-optical filters.
Inset: The calibrated temperature dependent joint spectrum of the p-polarized (blue) and s-polarized (purple) photons generated in the crystal when pumped with a 403,9 nm CW diode laser.
Taken from: R Whittaker et al 2017 New J. Phys. 19 023013

This approach works for a single mode. We might raise the question how we can realize imaging. For that the beams needs to be split into M pixels. We can do that by using M independent detectors. For a single-mode input beam this bounds the detection efficiency to $\eta \leq 1/M$.

We might also consider a multi-mode beam with one photon. However, for each single mode we would have super-Poissonian statistics, i. e. $F \geq 1$. this would give us no advantage.

We can use the SPDC to generate two correlated beams which can be used to perform a differential measurement. the measured quantity is then

$$\langle \hat{N}_- \rangle = \langle \hat{N}_2 - \hat{N}_1 \rangle = \alpha \langle \hat{n} \rangle . \tag{6.9}$$

The degree of correlation between the two modes is

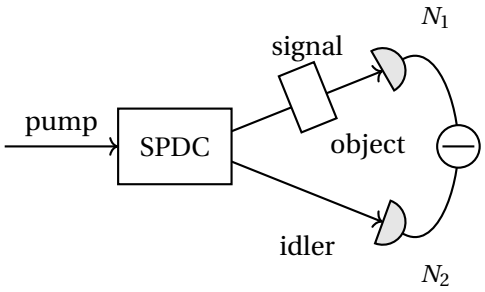

Fig. 28: Differential measurement using SPDC.

described by the *noise reduction factor*[3].

$$\sigma = \frac{\left\langle \Delta^2(\hat{N}_2 - \hat{N}_1)\right\rangle}{\left\langle \hat{N}_1 + \hat{N}_2\right\rangle} = \frac{\left\langle \Delta^2 \hat{N}_1\right\rangle + \left\langle \Delta^2 \hat{N}_2\right\rangle - 2\left\langle \Delta\hat{N}_1 \Delta\hat{N}_2\right\rangle}{\left\langle \hat{N}_1 + \hat{N}_2\right\rangle}. \tag{6.10}$$

In other words, σ describes how similar both beams are in their statistical parameters. This quantity is equivalent to the Fano factor for states in two modes for classical light $\sigma \geq 1$. Quantum correlations can lead to $0 \leq \sigma \leq 1$ affected by loss. If we assume same efficiency for both detectors $\eta_1 = \eta_2 = \eta$

$$\sigma_{\text{det}} = \eta\sigma + 1 - \eta \geq 1 - \eta. \tag{6.11}$$

Substituting (6.11) into equation (6.10) leads to

$$\left\langle \Delta^2 \hat{N}_- \right\rangle = \left[\alpha^2(F-1) + \alpha + 2\sigma(1-\alpha)\right] \langle \hat{n} \rangle . \tag{6.12}$$

With equation (6.2) the uncertainty of absorption becomes

$$\Delta\alpha_{\text{diff}} = \sqrt{\frac{\alpha^2(F-1) + \alpha + 2\sigma(1-\alpha)}{\langle \hat{n} \rangle}}. \tag{6.13}$$

For a weakly absorbing object $\alpha \ll 1$ we have $\alpha^2(F-1) \approx 0$ and with classical light ($\sigma = 1$) we find

$$\Delta\alpha_{\text{class.}} = \sqrt{\frac{2-\alpha}{\langle \hat{n} \rangle}}. \tag{6.14}$$

This is worse than a simple classical measurement. An improvement is only possible when using non-classical correlations

$$\frac{\Delta\alpha_{\text{diff}}}{\Delta\alpha_{\text{class.}}} = \sqrt{\frac{\alpha + 2\sigma(1-\alpha)}{(2-\alpha)}} \approx \sqrt{\sigma} \quad (\alpha \ll 1) \tag{6.15}$$

$$\frac{\Delta\alpha_{\text{diff}}}{\Delta\alpha} = \sqrt{\frac{\alpha + 2\sigma(1-\alpha)}{(1-\alpha)}} \approx \sqrt{2\sigma}. \tag{6.16}$$

We observe that for $\sigma < \frac{1}{2}$ the differential measurement is better than the ideal single measurement. This can now be applied to imaging, if strongly correlated multi mode beams are used.

Some experimental results of sub-shot-noise quantum imaging (SSNQI) are shown in figures 29 and 30.

[3] Note that $\left\langle \Delta^2 \hat{N}_1 \right\rangle \equiv (\Delta\hat{N})^2$

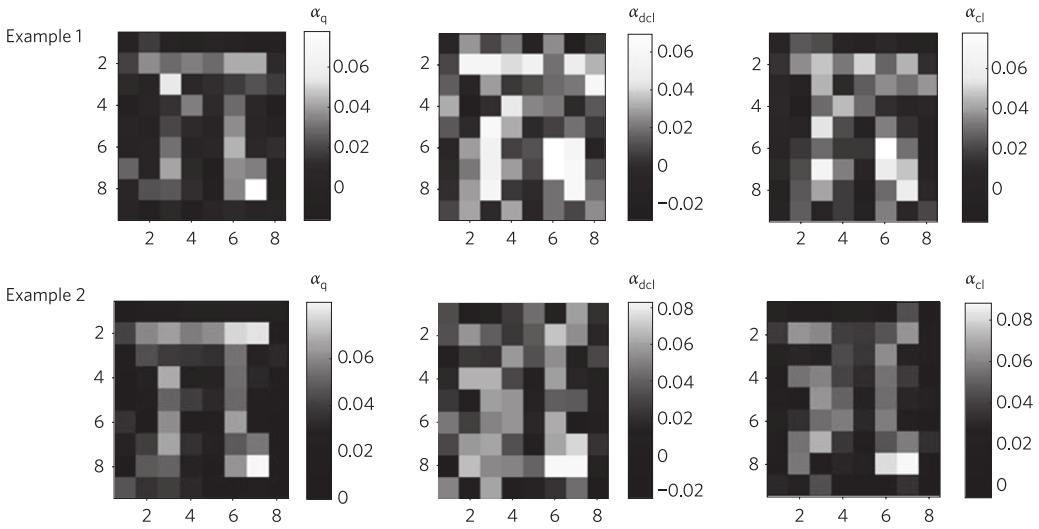

Fig. 29: Experimental imaging of a π-shaped titanium deposition with $\alpha = 0.5$ when $\sigma = 0.35$. Two sets of typical images are shown: SSNQI image (left), obtained by subtracting the quantum correlated noise; differential classical image (middle); direct classical image (right). The pixel size is $480\,\mu m^2$, obtained by fulfilling the condition $A_{pixel}/A_{coherence} \gg 1$ and reducing electronic noise. The mean number of photons per pixel is $\langle \hat{N} \rangle \approx 7000$.
Taken from: G Brida et al 2010, Nature Photon 4, 227-230.

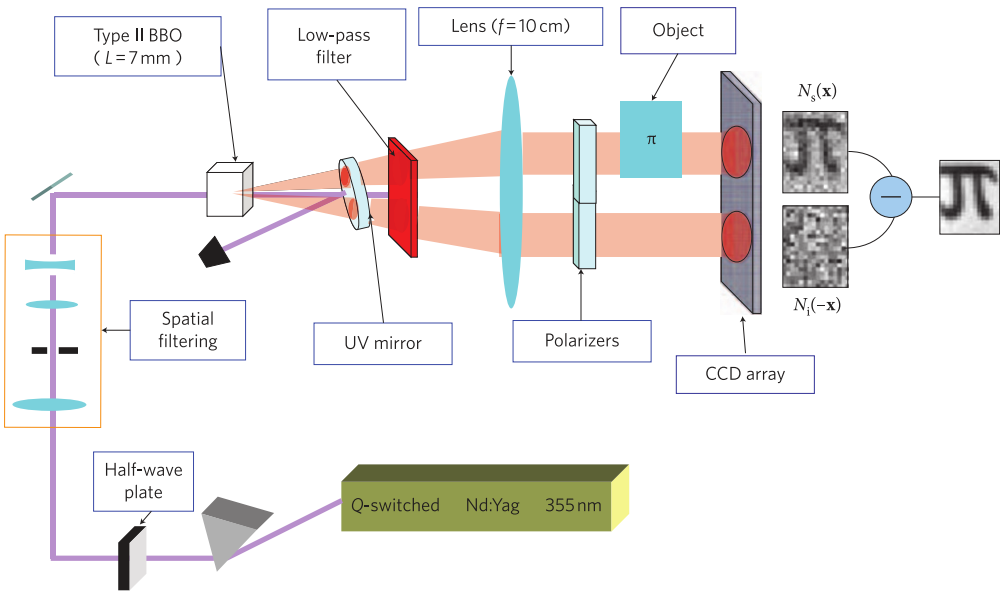

Fig. 30: Scheme of subshot noise imaging, where signal and idler photons are separated into two beams, one of which is transmitted through the object, and both of which are detected by a CCD camera.
Taken from: G Brida et al 2010, Nature Photon 4, 227-230.

6.2 Ghost Imaging

Now we again use an SPDC light source to create entangled photon pairs four our experiments. Detector D_2 (c. f. figure 31) detects only the arrival times of photons and does not image. Detector D_1 is an arrayed detector and does not see the object. Thus it also does not image the object. However, we can retrieve the image by performing correlation measurements. Here, the temporal correlation is used to identify signal/idler pairs. The spatial correlation is used to infer signal position on object from the idler measurement. For imaging we have to place a lens with

$$\frac{1}{f} = \frac{1}{s_1} + \frac{1}{d_1 + d_2}. \tag{6.17}$$

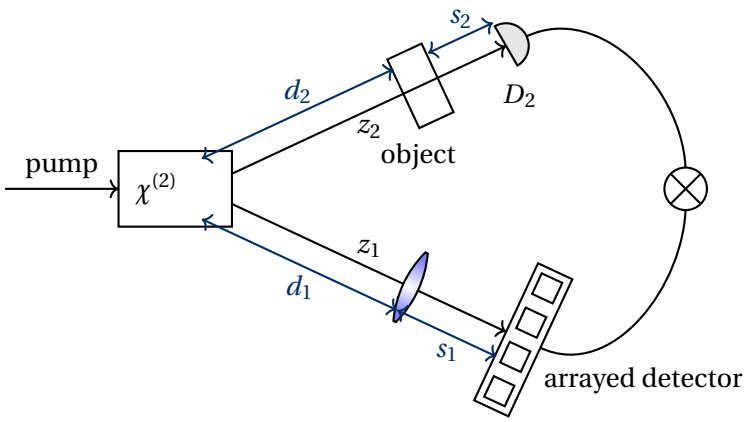

Fig. 31: Schematic drawing of an experimental setup used for Ghost Imaging.

Theoretical description

We assume only one transverse coordinate, which can be made general by using vectors for wave numbers $\boldsymbol{k}_n$ and coordinates $\boldsymbol{r}_n$.Furthermore we assume no polarization and a pump plane wave at normal incidence and the SPDC crystal. Thus the transverse wave number $\boldsymbol{k}_{\perp,p} \equiv \kappa_p = 0$ is zero. The generated two photon state is now given by

$$|\psi\rangle = C_0 \int \mathrm{d}\kappa_s \, \mathrm{d}\kappa_i \underbrace{\delta(\kappa_s + \kappa_i)}_{\text{momentum conservation}} \int \mathrm{d}\omega_i \, \mathrm{d}\omega_s \underbrace{\delta(\omega_i + \omega_s - \omega_p)}_{\text{energy conservation}} \hat{a}^\dagger(\kappa_s, \omega_s) \hat{a}^\dagger(\kappa_i, \omega_i) |0\rangle . \tag{6.18}$$

In the following we assume perfect phase matching. The measured signal is the correlations of the electric field

$$\begin{aligned} G^{(2)}(r_1, z_1, t_1; r_2, z_2, t_2) &= \left\langle \psi | \hat{E}_2^{(-)} \hat{E}_1^{(-)} \hat{E}_1^{(+)} \hat{E}_2^{(+)} | \psi \right\rangle \\ &= \left| \left\langle 0 | \hat{E}_2^{(-)} \hat{E}_1^{(+)} | \psi \right\rangle \right|^2 = |\psi(r_1, z_1, t_1; r_2 z_2, t_2)|^2. \end{aligned} \tag{6.19}$$

The different electric field are given by

$$\hat{E}_j(r_j, z_j, t) = \int \mathrm{d}\omega\, \mathrm{d}\kappa\, \mathrm{d}r_0\, h_j(\omega, r_j, r_0) \mathrm{e}^{-\mathrm{i}\omega t} \mathrm{e}^{-\mathrm{i}\kappa r_0}\, \hat{a}(\kappa_j, \omega). \tag{6.20}$$

r_0 is the coordinate at the source and h_j describes the transfer function. It relates the fields between different planes. Now putting the electric field and the states together we find

$$\begin{aligned}
\psi &= C_0 \int \mathrm{d}\kappa_s\, \mathrm{d}\kappa_i\, \delta(\kappa_i + \kappa_s)\, \mathrm{d}\omega_s\, \mathrm{d}\omega_i\, \delta(\omega_s + \omega_i - \omega_p) \\
&\quad \times \int \mathrm{d}\kappa_1\, \mathrm{d}\kappa_2\, \mathrm{d}\omega_1\, \mathrm{d}\omega_2\, \mathrm{d}r_0\, \mathrm{d}r_0'\, h_{z_1}(\omega_1, r_1, r_0)\, h_{z_2}(\omega_2, r_2, r_0') \\
&\quad \times \mathrm{e}^{-i(\omega_1 t_1 + \omega_2 t_2)} \mathrm{e}^{-i(\kappa_1 r_0 + \kappa_2 r_0')} \underbrace{\left\langle 0 | \hat{a}_1 \hat{a}_2 \hat{a}_s^\dagger \hat{a}_i^\dagger | 0 \right\rangle}_{} \\
&\quad = \delta(\omega_1 - \omega_s)\delta(\omega_2 - \omega_i)\delta(\kappa_1 - \kappa_s)\delta(\kappa_2 - \kappa_i) \\
&\qquad + \delta(\omega_1 - \omega_i)\delta(\omega_2 - \omega_s)\delta(\kappa_1 - \kappa_i)\delta(\kappa_2 - \kappa_s) \\
\psi &= 2C_0 \int \mathrm{d}\kappa_s\, \mathrm{d}\kappa_i\, \mathrm{d}\omega_i\, \mathrm{d}\omega_s\, \mathrm{d}r_0\, \mathrm{d}r_0' \underbrace{\mathrm{e}^{-i(\omega_s t_1 + \omega_i t_2)} \mathrm{e}^{-i(\kappa_s r_0 + \kappa_i r_0')}}\, h_{z_1}(\omega_s, r_1, r_0)\, h_{z_2}(\omega_i, r_2, r_0) \\
&\qquad \mathrm{e}^{-\mathrm{i}\omega_p t_1} \mathrm{e}^{-\mathrm{i}\omega_s (t_1 - t_2)} \mathrm{e}^{-\mathrm{i}\kappa_s (r_0 - r_0')} \\
&= 2C_0 (2\pi)^3 \delta(t_1 - t_2) \mathrm{e}^{-\mathrm{i}\omega_p t_1} \underbrace{\int \mathrm{d}r_0\, h_{z_1}(r_1, r_0)\, h_{z_2}(r_2, r_0)}_{\Phi(r_1, z_1; r_2, z_2)}.
\end{aligned} \tag{6.21}$$

If we now assumed that $\omega_s = \omega_i = \omega$ we can drop the frequency argument. The object is completely contained in the transfer function $h_{z_2}(r_2, r_0)$

$$h_{z_2}(r_2, r_0, z_2) = \int \mathrm{d}r\, h_{s_2}(r_2, r) \underbrace{T(r)}_{\text{transmission of the object}} h_{d_2}(r, r_0). \tag{6.22}$$

Now we redistribute the transfer functions and define

$$\begin{aligned}
h_0(r_1, r) &= \int \mathrm{d}r_0\, h_{z_1}(r_1, r_0)\, h_{d_2}(r, r_0) \quad \text{relates } D_2 \text{ to object plane.} \\
\Phi &= \int \mathrm{d}r\, h_0(r_1, r)\, T(r)\, h_{s_2}(r_2, r).
\end{aligned} \tag{6.23}$$

For coincidences we again consider $G^{(2)}$

$$G^{(2)}(r_1, z_1; r_2, z_2) = \Phi\Phi^* = \int \mathrm{d}r\, \mathrm{d}r'\, h_0(r_1, r)\, h_0^*(r_1, r')\, T(r)\, T^*(r')\, h_{s_2}(r_2, r)\, h_{s_2}^*(r_2, r'). \tag{6.24}$$

We find correlations between the coordinates r_1, r_2 in the detector planes. Finally detector 2 integrates over all photons. We call that a *bucket detector*. The coincidence rate is now given as

$$R_c(r_1) = \int \mathrm{d}r_2\, G^{(2)}(r_1, z_1; r_2, z_2) = \int \mathrm{d}r\, \mathrm{d}r' \underbrace{h_0(r_1, r)\, h_0^*(r_1, r')}_{\text{object to } D_1}\, T(r) \underbrace{g(r, r')}_{\text{object to } D_2} \tag{6.25}$$

$$\text{where} \quad g(r, r') = \int \mathrm{d}r_2\, h_{s_2}(r_2, r)\, h_{s_2}^*(r_2, r'). \tag{6.26}$$

The correlation counts are proportional to the transmission of the object. Depending on $g(r, r')$, different types of imaging can be implemented:

- If $g(r,r') = \delta(r-r') \quad \Rightarrow \quad R_c(r_1) = \int \mathrm{d}r\, |h_0(r_1,r)T(r)|^2$.
  In each detector point, intensities from the object are summed up. This corresponds to incoherent imaging. This can be realized with a $2f$ or $4f$-system between object and D_2.
- if $g(r,r') = f^*(r)\cdot f(r')$ (factorizable) we have

$$R_c(r_1) = \left| \int \mathrm{d}r\, h_0(r_1,r)T(r)f(r) \right|^2. \tag{6.27}$$

  Here, different object contributions are coherently summed up. This leads to coherent imaging which can be reached, if h_{s_2} does not depend on r_2, e. g. if the detector is very far from the object.

In both cases, the detection rate is proportional to the object transmission. The path h_2 influences imaging similar to a classical source. A sharp image can be obtained if h_0 satisfies the imaging condition.

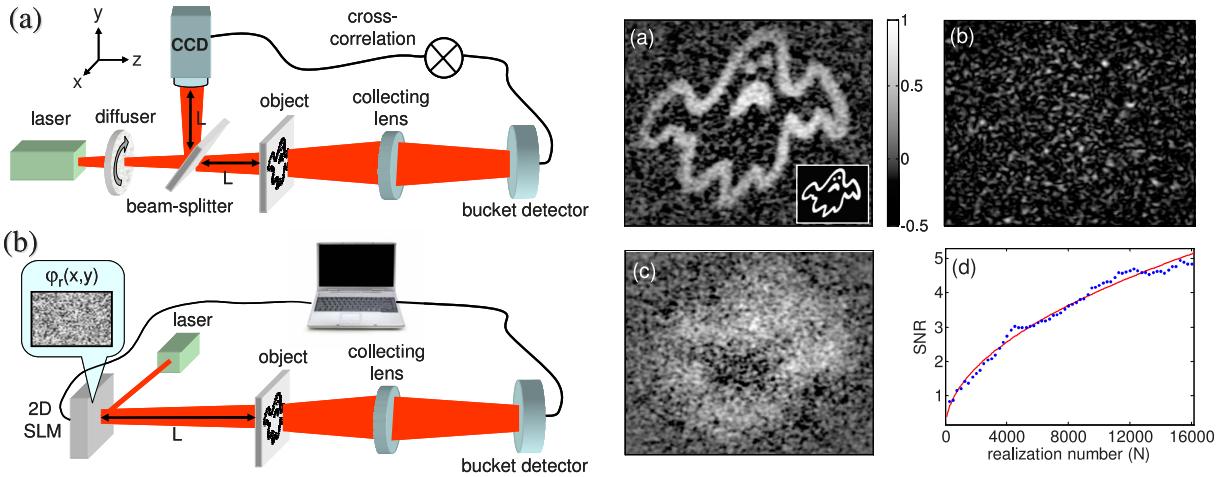

Fig. 32: Left: Experimental setups for Ghost Imaging. (a) The standard two-detector setup, where the image of the object is obtained by correlating the pseudothermal field measured by a CCD with the intensity measured by a bucket detector. (b) The computational single-detector setup used here. The light beam is generated by a spatial light modulator (SLM). The intensity measured by the bucket detector is correlated with the calculated field at the object plane.
Right: Computational Ghost Image reconstruction of a 4 cm^2 mask. (a) reconstructed image, obtained with 16000 realizations. (b) Calculated intensity pattern of a single phase realization. (c) Reconstructed out-of-focus image at a different plane demonstrating depth resolving capabilities. (d) measured SNR or the reconstructed image. The theoretical line depicts $\sqrt{N}$ dependence.
Taken from: Bromberg et al., Phys. Rev. A 79, 053840 (2009)

6.3 Inverse classical representation of Ghost Imaging

In the mathematical description, h_0 has the role of a propagator/transfer function between object and imaging detector. $g(r,r')$ and the detector D_2 influence the image like a light source. Therefore all spatial properties of Ghost Imaging can be explained with a classical analogue as depicted in figure 33. The classical analogue imaging scheme results in the

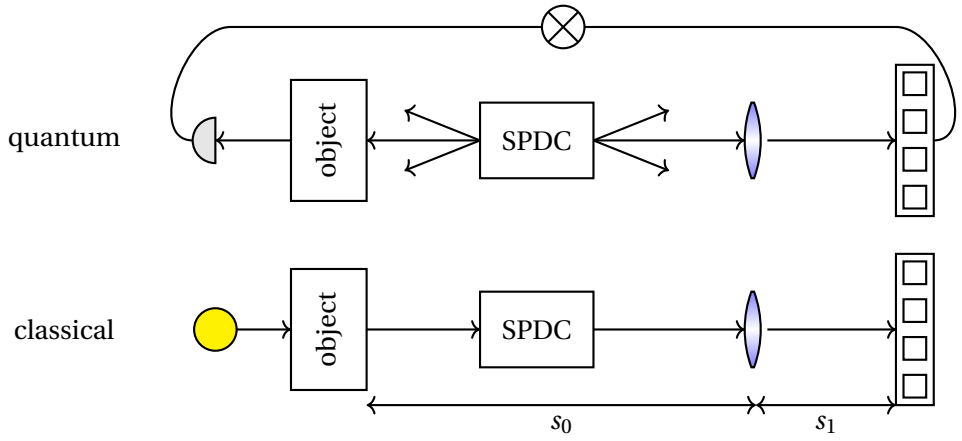

Fig. 33: Comparison between a quantum and classical Ghost Imaging scheme.

same image as Ghost Imaging with a plane-wave pump and degenerate signal and idler. The imaging condition states

$$\frac{1}{f} = \frac{1}{s_0} + \frac{1}{s_1}. \tag{6.28}$$

We conclude that Ghost Imaging can also be done with classical light.

In figure 34 we can see a scheme for classical Ghost Imaging. The diffuser generates a temporally varying random speckle pattern. The image is obtained by correlating the camera frames with the detector measurement. It is import to note that for Ghost Imaging only spatial correlations are needed, non-classical entanglement is not necessary.

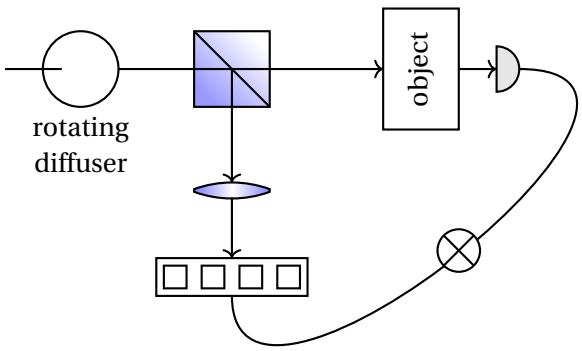

Fig. 34: Ghost Imaging with classical light.

Why do we need quantum Ghost Imaging?

Quantum Ghost Imaging is using photon pairs to illuminate the object, because there is a perfect correlation between signal and idler. This leads to a better signal-to-noise ratio (SNR)

$$G = \frac{\mathrm{SNR}_{\mathrm{SPDC}}}{\mathrm{SNR}_{\mathrm{class}}} = \frac{1}{\mu} + 1, \tag{6.29}$$

where μ is the number of photons per pixel on the array detector. Quantum Ghost Imaging is interesting for applications where the intensity is limited. Furthermore Quantum Ghost Imaging can be implemented with different signal/idler wavelengths. For example, imaging can be done at an accessible wavelength range, you only need a single detector for more complicated wavelength that measures the object.

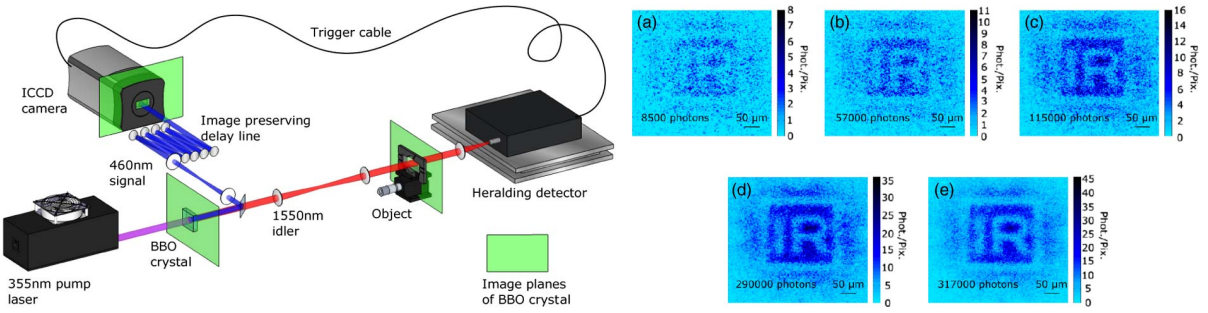

Fig. 35: Left: Experimental setup. The non-degenerate SPDC process generates a visible/IR photon pair at the BBO crystal which is split at a dichroic mirror. The IR photon probes an object and the transmitted photons are detected by a single-element heralding detector. The detection event triggers the ICCD camera, which detects the delayed visible photon. The recovered image of the object is the accumulation of many visible photon detections by the ICCD.
Right: Image of a test object. A stencil of the letter "IR" obtained in visible light by an ICCD camera, even though the object was illuminated by IR only.
Taken from: Aspden et al., Optica 2, 1049 (2015).

7 Quantum microscopy

7.1 Correlation super resolution imaging

Up to now, only one photon interacted with the object. We concluded, that here the resolution is the quantum case is the same in a classical measurement. Now we raise the question what happens, if both photons of a pair interact with the object.

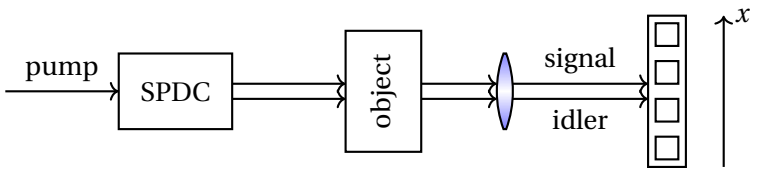

Fig. 36: Imaging experiment where both signal and idler interact with the object. We assume both photons to have the same wavelength.

The corresponding schematic for an experiment is sketched in figure 36. The lens ensures the imaging condition between object and detector. For each photon, each point on the object leads to a distribution of detection events.

The detection events are random and independent for signal and idler. This leads to a distribution on the detector. Mathematically this can be described by a point-spread function (PSF). Classically, the width of the PSF limits the resolution and corresponds to the variance of position of signal and idler photons

$$\Delta^2 \delta x_s = \Delta^2 \delta x_i = (\sigma_{\mathrm{PSF}})^2. \tag{7.1}$$

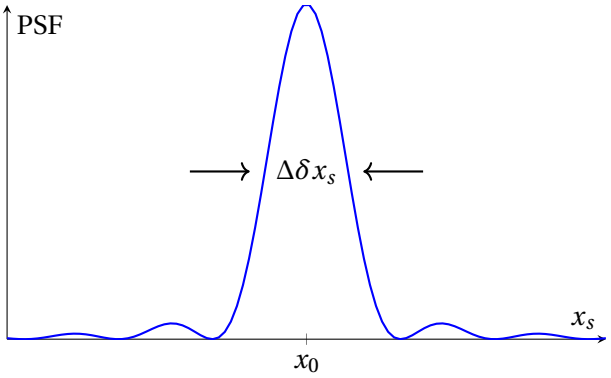

Fig. 37: Point-spread function

Here, $\Delta^2 \delta x_s$ corresponds to the distance between the detected position of the signal photon and their incident position in the object plane. The centroid of positions of both photons is given by

$$\delta x_c = \frac{\delta x_i + \delta x_s}{2}. \tag{7.2}$$

The uncertainty of the centroid measurement is

$$r = \sqrt{\Delta^2 \delta x_c} = \sqrt{\Delta^2 \frac{\delta x_i + \delta x_s}{2}} = \frac{\sqrt{\Delta^2 (\delta x_i + \delta x_s)}}{2}, \quad \text{where} \quad \Delta^2 (a \cdot x) = a^2 \Delta^2 x. \tag{7.3}$$

The quantities δx_i and δx_s are normally distributed, independent random variables, because they interact independently with the diffracting object. Thus the variance of the sum is simply the sum of variances

$$r = \frac{1}{2} \sqrt{\Delta^2 \delta x_i + \Delta^2 \delta x_s} = \frac{\sigma_{\mathrm{PSF}}}{\sqrt{2}}. \tag{7.4}$$

this improves the resolution by a factor of $1/\sqrt{2}$. We can implement this by using arrays of single-photon detectors of sensitive cameras. Every frame of measurement can contain only a small number of photon pairs, so that the centroid can be estimated. This works in principle also for higher photon number N. The resolution would improve by $1/\sqrt{2N}$, however, so far no good sources for such states exist.

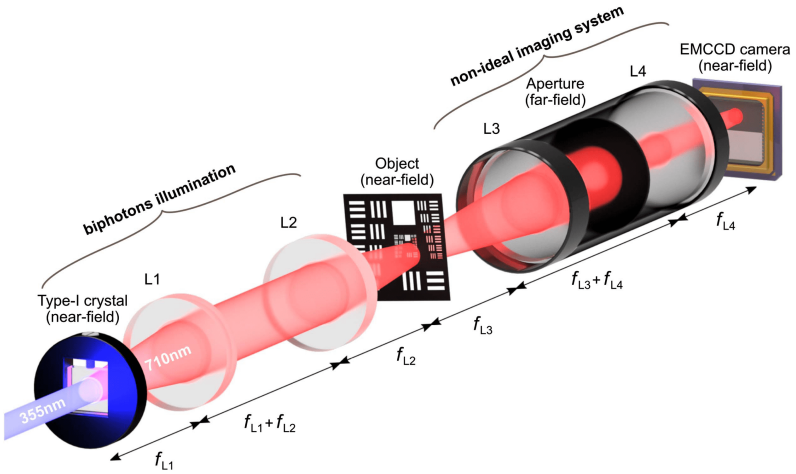

Fig. 38: Experimental setup. The optics consists of a source of spatially correlated photons (biphoton illumination), an object, a non-ideal imaging system and a single-photon EMCCD camera. The planes of crystal and object are imaged onto the plane of the detector. An aperture in the far field is used to tune the diffraction limit.
Taken from: Toninelli et al., Optica 3, 347 (2019).

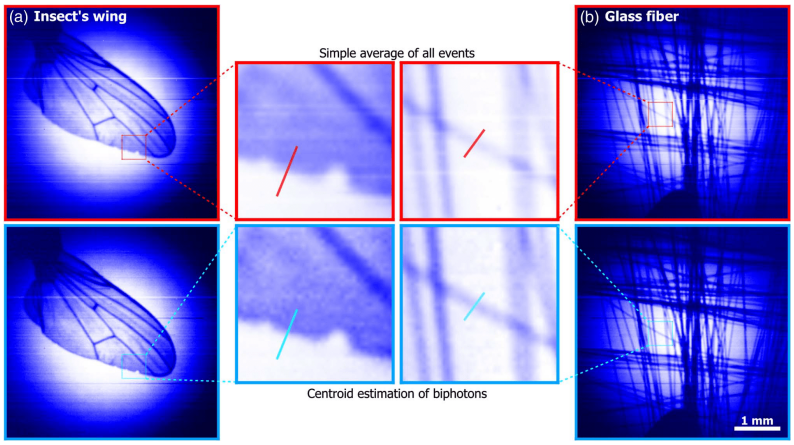

Fig. 39: Image comparison for real-world objects. The wing of a fly (a) and glass fibers (b) were imaged using the single average of all frames (top row) and the centroid estimation of biphotons (bottom row). The horizontal streak lines are due to an uneven response of regions of the EMCCD chip and to charge smearing.
Taken from: Toninelli et al., Optica 3, 347 (2019).

7.2 Fluorescence correlation imaging

Most high-end microscopes are based on fluorescence. Fluorophores are emitters of non-classical light (single photon states). The single photons show distinct properties in correlation measurements, namely anti-bunching. We raise the question whether or not correlation measurements can improve the imaging resolution. We want to check if it can enable to determine positions of closely spaced emitters.

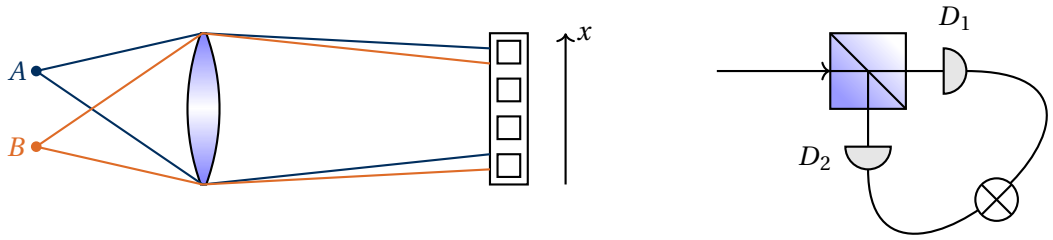

Fig. 40: Point spread function of closely space emitters on a detector.

Let $P(x)$ be the probability to detect a photon from a single emitter at position x. We now use a beam splitter with $T+R=1$. Then the single count intensities are

$$I_1^{D_1}(x) = T(P_A(x)+P_B(x)) \quad \text{and} \quad I_1^{D_2}(x) = R(P_A(x)+P_B(x)). \tag{7.5}$$

The sum of both detector intensities will be the sum of both probabilities $I_1(x) = P_A(x) + P_B(x)$. If A and B are close together, the Airy-function of P_A and P_B will overlap and may not be distinguished. A correlation measurement measures the probability for two photons to arrive simultaneously. It will be zero if only one emitter contributes and nonzero in overlapping regions. The correlations counts are characterized by

$$I_2(x) = RTP_A(x)P_B(x). \tag{7.6}$$

From I_1 and I_2 we can calculate P_A and P_B if R, T are known quantities. Here we assume that only two fluorophores contribute at any position. However, this can be expanded to higher number of emitters. Unfortunately more detectors are needed for this.

We can discuss the problem more generally in terms of point spread functions (PSF). Measuring $[P(x)]^k$ reduces the width by $\sqrt{k}$. We want to answer the question how we can use this with single emitters. An ensemble of n emitters produces a signal

$$s \sim \sum_{\alpha=1}^{n} P_\alpha(x) \quad \text{what we need is:} \quad \sum_{\alpha=1}^{n} (P_\alpha(x))^k. \tag{7.7}$$

Simply taking the k-th power of signal s is not suited since it contains cross products of different emitters. We can mathematically describe the signal using the expectation value of the photon number operator for a given measurement configuration at position x

$$\langle \hat{N} \rangle = \sum_{\alpha=1}^{n} P_\alpha(x) \quad \text{with} \quad \hat{N} = \sum_{\alpha=1}^{n} \hat{a}_\alpha^\dagger \hat{a}_\alpha. \tag{7.8}$$

Then the k-th order correlation function $g^{(k)}(t=0)$ is

$$g^{(k)} = \frac{\left\langle \prod_{i=0}^{k-1}(\hat{N}-i)\right\rangle}{\left\langle \hat{N}\right\rangle^k}$$
$$g^{(2)} \overset{k=2}{=} \frac{\left\langle \hat{a}^\dagger\hat{a}^\dagger\hat{a}\hat{a}\right\rangle}{\left\langle \hat{a}^\dagger\hat{a}\right\rangle^2} = \frac{\left\langle \hat{a}^\dagger(\hat{a}\hat{a}^\dagger-1)\hat{a}\right\rangle}{\left\langle \hat{a}^\dagger\hat{a}\right\rangle^2} = \frac{\left\langle \hat{N}^2-\hat{N}\right\rangle}{\left\langle \hat{N}\right\rangle^2}. \tag{7.9}$$

We can express the needed measurements with the correlation function (first for two emitters)

$$\sum_{\alpha=1}^{2}(P_\alpha(x))^2 = \left\langle \hat{N}\right\rangle^2(1-g^{(2)}) = \left\langle \hat{N}\right\rangle^2 - \left\langle \hat{N}^2-\hat{N}\right\rangle. \tag{7.10}$$

To calculate the expectation values, we need an explicit representation of the state $\left|\psi\right\rangle$

$$\left|\psi\right\rangle = \sqrt{P_AP_B}\left|1,1\right\rangle + \sqrt{P_A(1-P_B)}\left|1,0\right\rangle + \sqrt{(1-P_A)P_B}\left|0,1\right\rangle + \sqrt{(1-P_A)(1-P_B)}\left|0,0\right\rangle, \tag{7.11}$$

where $P_{A,B}$ are the probabilities to collect photons from each emitter. Now the expectation value of the number operator $\hat{N} = \hat{a}_A^\dagger\hat{a}_A + \hat{a}_B^\dagger\hat{a}_B$ is

$$\left\langle\psi|\hat{N}|\psi\right\rangle = p_AP_B + P_A(1-P_B) + P_AP_B + (1-P_A)P_B = P_A + P_B \tag{7.12}$$
$$\Rightarrow \left\langle \hat{N}\right\rangle^2 = P_A^2 + P_B^2 + 2P_AP_B. \tag{7.13}$$

Correspondingly we can calculate $\left\langle \hat{N}^2\right\rangle$

$$\left\langle \hat{N}^2\right\rangle = \left\langle (\hat{a}_A^\dagger\hat{a}_A + \hat{a}_B^\dagger\hat{a}_B)^2\right\rangle = 2P_AP_B + P_A + P_B. \tag{7.14}$$

Substituting this into (7.10) yields

$$\sum_{\alpha=1}^{2}(P_\alpha(x))^2 = \left\langle \hat{N}\right\rangle^2 - \left\langle \hat{N}^2-\hat{N}\right\rangle = P_A^2 + P_B^2, \tag{7.15}$$

which is exactly what we wanted. We also want to refer to an experiment conducted by Cui et al. in 2013. They performed an experiment on fluorescence correlation imaging using two photons. The setup is displayed in figure 41. The experimental results are displayed in figure 42.

It is also possible to generalize this approach for higher orders, e. g. $k=3$

$$\sum_{\alpha=1}^{3}(P_\alpha(x))^3 = \left\langle \hat{N}\right\rangle^3\left(1-\frac{3}{2}g^{(2)}+\frac{1}{2}g^{(3)}\right). \tag{7.16}$$

When we can obtain correlation measurements of higher orders, we can also calculate higher powers of the PSF. Furthermore, if we know that higher orders of $g^{(k)}$ are zero we can also calculate higher order powers of P^k. With that we can further increase the imaging resolution, however, we need to use a-priori information about the object.

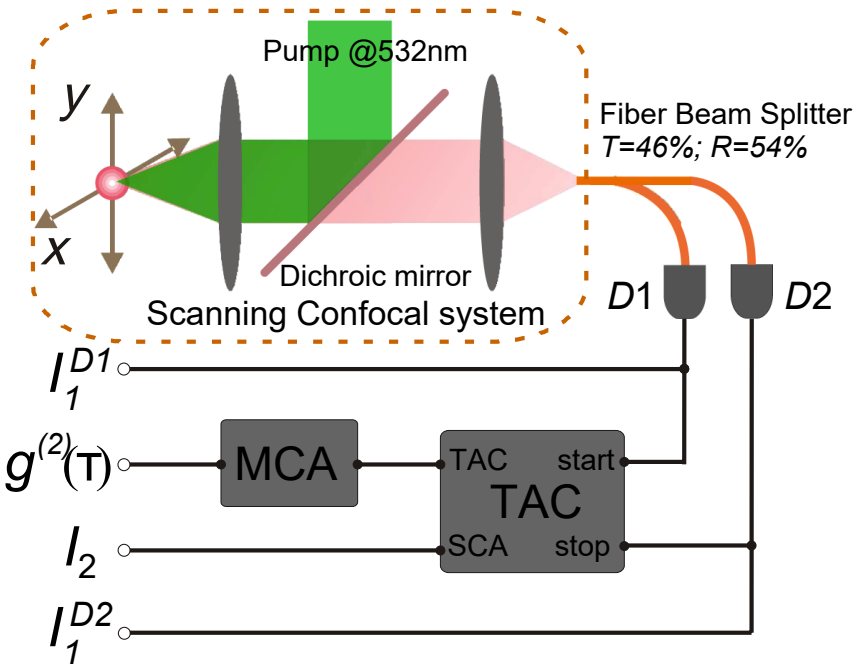

Fig. 41: Schematic of the measurement setup. Confocal (nitrogen vacancy) fluorescent photons are split by a fiber BS and sent to single photon detectors D_1 and D_2. A time-amplitude converter (TAC) is used to get coincidence count and a multi channel analyzer (MCA) to implement the autocorrelation measurement $g_c^{(2)}(\tau)$.
Taken from: Cui et al., Phys. Rev. Lett. 110, 153901 (2013)

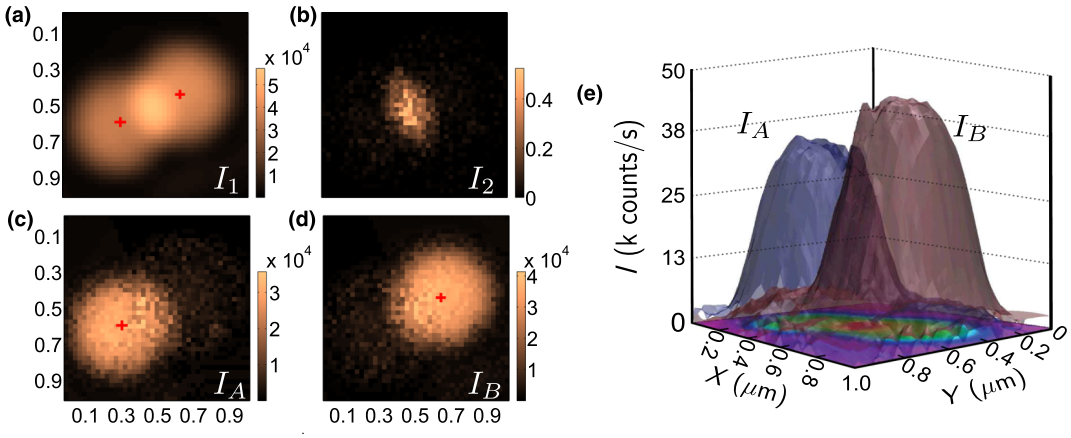

Fig. 42: Optical images of two single (nitrogen vacancy centres) NVC at a distance of 366 nm. I_1 and I_2 are the single-photon and two-photon counts. The red crosses mark the positions of the NVcs. The positions were obtained by using a 2D Gaussian fitting.
Taken from: Cui et al., Phys. Rev. Lett. 110, 153901 (2013)

7.3 Multi-photon quantum microscopy

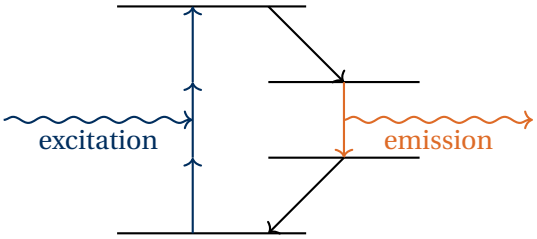

Fig. 43: multi photon absorption in a molecule.

Multi-photon microscopy is also often called fluorescence microscopy. It utilizes the multi-photon absorption of a molecule emitting a single photon. The final resolution depends on detection (which was discussed before) and excitation. The excitation spot is limited by the diffraction limit (Airy-disc). The diameter in excitation can be reduced when using correlations. Here, fluorophores act as a detector that measures correlations. We may use an excitation laser of longer wavelength. Then, two or more photons are needed for excitation. It only works if the photons arrive at the same time, thus we have a correlation *measurement*.

The emission probability is proportional to

$$P_{\text{emission}} \sim |I_{\text{exc.}}(x)|^n, \tag{7.17}$$

where n is the photon number.

The Airy function $I(x)$ is leading to a narrower distribution of excitation, the width reduces by a factor $\sqrt{n}$. Classically, photons are randomly distributed. Then the excitation probability scales quadratically with intensity. In photon pairs, two photons always appear together. Thus, with correlated pairs, emission can be enhanced for small excitation intensity as sketched in figure 44.

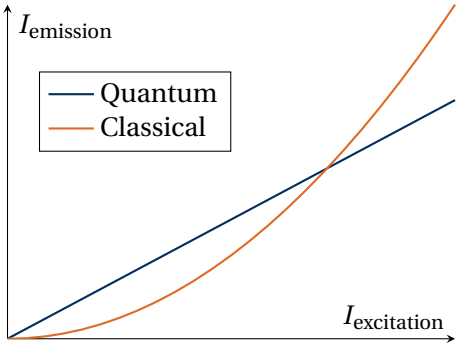

Fig. 44: Emission probability for classical and non-classical photons.